



# Contents

<b>1</b>	<b>Introduction</b>	<b>3</b>
<b>2</b>	<b>Deep-inelastic scattering with QED corrections</b>	<b>6</b>
2.1	QED corrections to PDF evolution . . . . .	6
2.2	Fitting PDFs with QED corrections . . . . .	8
2.3	The photon PDF from DIS data . . . . .	10
<b>3</b>	<b>The photon PDF from <math>W</math> and <math>Z</math> production at the LHC</b>	<b>15</b>
3.1	The prior NNPDF2.3QED and its reweighting . . . . .	16
3.2	The NNPDF2.3QED set . . . . .	21
<b>4</b>	<b>Implications for HERA and LHC phenomenology</b>	<b>28</b>
4.1	Direct photon production at HERA . . . . .	28
4.2	Searches for new massive electroweak gauge bosons . . . . .	29
4.3	$W$ pair production at the LHC . . . . .	31
<b>5</b>	<b>Conclusions</b>	<b>34</b>

# 1 Introduction

Because of the need for precision phenomenology at the LHC [1, 2] the parton distributions (PDFs) of the nucleon are currently determined using next-to-next-to leading order (NNLO) QCD. At this level of accuracy, however, electroweak (EW) corrections also become relevant, and indeed EW corrections to various hadron collider processes have been studied in detail, such as for instance inclusive  $W$  and  $Z$  production [3–13],  $W$  and  $Z$  boson production in association with jets [14–16], dijet production [17, 18] and top quark pair production [19–23].

A consistent inclusion of EW corrections, however, requires the use of PDFs which incorporate QED effects. This in particular implies the inclusion of QED corrections to perturbative evolution, and thus a photon PDF. There is currently only one PDF set with QED corrections available, the MRST2004QED set [24]. In this pioneering work, the photon PDF was determined based on a model inspired by photon radiation off constituent quarks (though consistency with some HERA data was checked a posteriori), and therefore not provided with a PDF uncertainty.

In this work we will construct a PDF set including QED corrections, with a photon PDF parametrized in the same way as all the other PDFs, and determined from a fit to hard-scattering experimental data. Our goal is to construct a PDF set with the following features:

- QCD corrections included up to NLO or NNLO;
- QED corrections included to LO;
- a photon PDF obtained from a fit to deep-inelastic scattering (DIS) and Drell-Yan (both low mass, on-shell  $W$  and  $Z$  production, and high mass) data;
- all other PDFs constrained by the same data included in the NNPDF2.3 PDF determination [25].

The lepton PDF, as well as weak contributions to evolution equations [26, 27] are negligible and will not be considered here.

In principle, this goal could be achieved by simply performing a global fit including QED and QCD corrections both to perturbative evolution and to hard matrix elements, and with data which constrain the photon PDF. In practice, this would require the availability of a fast interface, like `APPLgrid` [28] or `FastNLO` [29], to codes which include QED corrections to processes which are sensitive to the photon PDF, such as single or double gauge boson production. Because such interfaces are not available, we adopt instead a reweighting procedure, which turns out to be sufficiently accurate to accommodate all relevant existing data.

The reweighting procedure we use works as follows (see Fig. 1). First, we construct a set of PDFs (NNPDF2.3QED DIS-only), including a photon PDF, by performing a fit to deep-inelastic scattering (DIS) data only, based on the same DIS data used for NNPDF2.3, and using either NLO or NNLO QCD and LO QED theory. To leading order in QED, the photon PDF only contributes to DIS through perturbative evolution (just like the gluon PDF to leading order in QCD). Therefore, the photon PDF is only weakly constrained by DIS data, and thus the photon PDF in the NNPDF2.3QED DIS-only set is affected by

large uncertainties. The result is a pair of PDF sets: NNPDF2.3QED DIS-only, NLO or NNLO, according to how QCD evolution has been treated.

In the next step, each replica of the photon PDF from the NNPDF2.3QED DIS-only set is combined with a random PDF replica of a set of the default NNPDF2.3 PDFs, fitted to the global dataset. This works because of the small correlation between the photon PDF and other PDFs, as we shall explicitly check. Also, the violation of the momentum sum rule that this procedure entails is not larger than the uncertainty on the momentum sum rule in the global QCD fit. The procedure is performed using NLO or NNLO NNPDF2.3 PDFs, for three values of  $\alpha_s(M_z) = 0.117, 0.118, 0.119$ . The photon PDF determined in the NNPDF2.3QED DIS-only fit is in fact almost independent of the value of  $\alpha_s$  within this range. This leads to several sets of PDF replicas, which we call NNPDF2.3QED prior, at the scale  $Q_0$ . The NNPDF2.3QED prior PDFs are then evolved to all  $Q^2$  using combined QCD+QED evolution equations, to LO in QED and either to NLO or NNLO in QCD and with the appropriate value of  $\alpha_s$ .

The LHC  $W$  and  $Z/\gamma^*$  production data are now included in the fit by Bayesian reweighting [30] of the NNPDF2.3QED prior PDF set. The set of reweighted replicas is then unweighted [31] in order to obtain a standard set of 100 replicas of our final NNPDF2.3QED set.

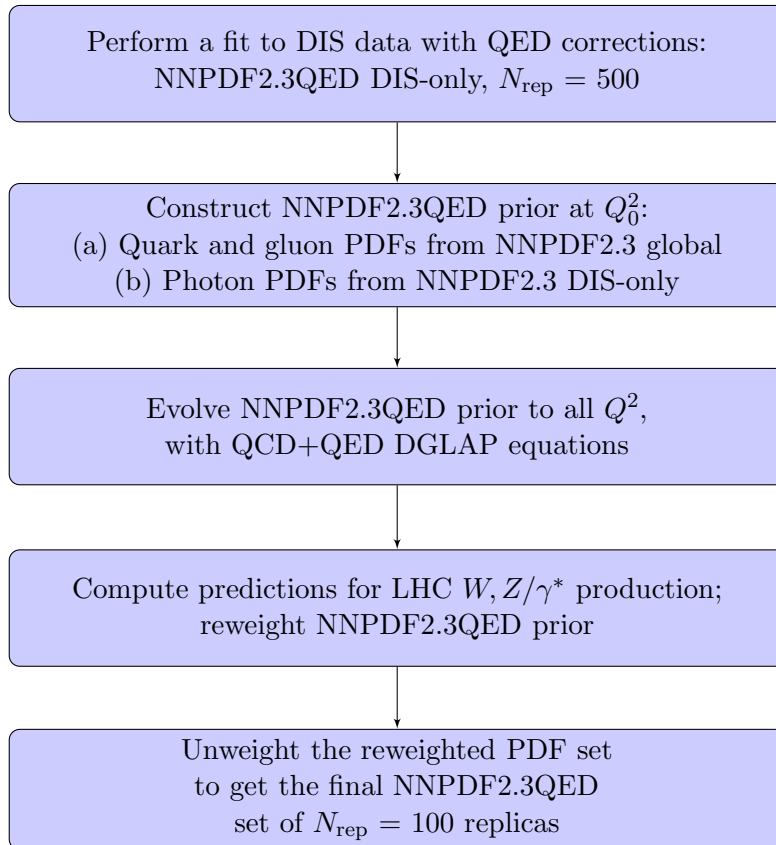


Figure 1: Flow-chart for the construction of the NNPDF2.3QED set.

The photon PDF in our final set turns out to be in good agreement with that from the MRST2004QED set at medium large  $x \gtrsim 0.03$ , while for smaller  $x$  values it is substantially smaller (by about a factor three for  $x \sim 10^{-3}$ ), though everywhere affected by sizable uncertainties, typically of order 50%. We will perform some first illustrative phenomenological studies using the NNPDF2.3QED set, and in particular discuss deep-inelastic direct photon production at HERA, photon-induced corrections to backgrounds in  $W'$  and  $Z'$  searches and electroweak corrections to vector boson pair production.

The paper is organized as follows. In Sect. 2 we present the implementation in the NNPDF framework of combined QCD and QED evolution equations, and its comparison with publicly available QED evolution codes. In Sect. 2 we also discuss the first step of our procedure, namely, the determination of NNPDF2.3QED DIS-only PDF set. The subsequent steps, namely the construction of the NNPDF2.3QED prior set, and its reweighting and unweighting leading to the final NNPDF2.3QED set are presented in Sect. 3. Finally, our phenomenological investigations are presented in Sect. 4.

## 2 Deep-inelastic scattering with QED corrections

The first step of our procedure is to perform a PDF fit to DIS data in which QED corrections are included to leading order. This requires solving the perturbative evolution equations which combine QED and QCD collinear radiation. We first review our implementation of combined QED+QCD evolution in the NNPDF perturbative evolution framework, in particular using the `FastKernel` method first presented in Ref. [32], and then turn to the PDF determination.

### 2.1 QED corrections to PDF evolution

The resummation of collinear singularities related to QED radiation through the solution of QED evolution equations, and its combination with QCD evolution equations has been understood for many years [33–35]: collinear photon radiation from charged leptons or quarks leads to a scale dependence which has the same structure as that of QCD evolution. At leading order the  $P_{qq}$ ,  $P_{q\gamma}$  and  $P_{\gamma q}$  splitting functions coincide with their  $P_{qq}$ ,  $P_{qg}$  and  $P_{gq}$  counterparts, up to the value of the coupling, which in QED is proportional to the square of the electric charge. Because there is no photon self-coupling, the  $P_{\gamma\gamma}$  splitting function only receives contributions from self-energy virtual corrections, and is thus proportional to a  $\delta(1-x)$ . The combined QCD+QED evolution equations thus take the form

$$Q^2 \frac{\partial}{\partial Q^2} f(x, Q^2) = \left[ \frac{\alpha(Q^2)}{2\pi} P^{\text{QED}} + \frac{\alpha_s(Q^2)}{2\pi} P^{\text{QCD}} \right] \otimes f(x, Q^2), \quad (1)$$

where  $f(x, Q^2)$  is a vector which includes all parton distributions,  $P^{\text{QED}}(x)$  and  $P^{\text{QCD}}(x)$  are respectively QED and QCD matrices of splitting functions, which admit respectively an expansion in powers of the fine structure constant  $\alpha$  and the strong coupling  $\alpha_s$ , and  $\otimes$  denotes the standard convolution.

A priori, the vector  $f(x, Q^2)$  includes quark, gluon, lepton and photon PDFs. In practice, however, the lepton PDFs of the nucleon are negligibly small, and may be safely neglected: thus we will take  $f(x, Q^2)$  to include the usual parton PDFs and a photon PDF  $\gamma(x, Q^2)$ . The combined QED+QCD evolution equations can be solved as usual by taking a Mellin transform, whereby they reduce to coupled ordinary differential equations. It is easy to check that the QCD and QED splitting function matrices do not commute. However, their commutator is of order  $\alpha\alpha_s$ , which is subleading. It follows that, up to  $O(\alpha\alpha_s)$  corrections, the solution can be written in factorized form as

$$f_i(N, Q^2) = \Gamma_{ik}^{\text{QCD}}(N, Q^2, Q_0^2) \Gamma_{kj}^{\text{QED}}(N, Q^2, Q_0^2) f_j(N, Q_0^2), \quad (2)$$

where  $f(N, Q^2)$  is the Mellin transform of the vector of parton distributions  $f(x, Q^2)$ , and  $\Gamma_{ik}^{\text{QCD}}(N, Q^2, Q_0^2)$  and  $\Gamma_{ik}^{\text{QED}}(N, Q^2, Q_0^2)$  are respectively the evolution kernels which solve the QCD and QED evolution equations.

We have implemented a combined solution of the QED+QCD evolution equations based on Eq. (2) in the NNPDF code, using the `FastKernel` method of Ref. [32], and with leading-order running of the fine structure constant. Details of the implementation will be given in a separate publication [36].

Previous numerical implementations of combined QED and QCD evolution were presented in Refs. [24, 37, 38], and specifically in Ref. [38] a public code (`partonevolution`)

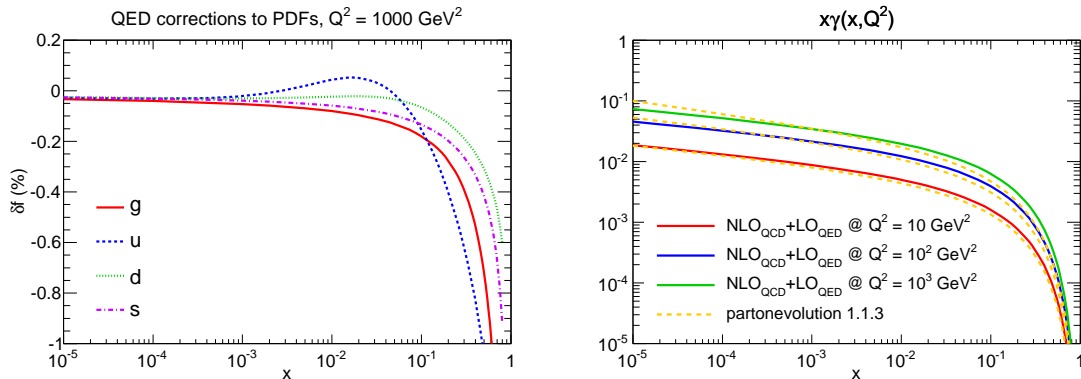


Figure 2: Left: relative difference between PDFs obtained from pure NLO QCD evolution and QCD NLO + QED LO evolution at  $Q^2 = 10^3 \text{ GeV}^2$ . Right: dynamically generated photon PDF at  $Q^2 = 10, 10^2$  and  $10^3 \text{ GeV}^2$ ; the result obtained using the `partonevolution` code of Ref. [38, 40] is also shown (dashed curves).

for the solution of combined evolution equations to leading order in the QED coupling and up to next-to-leading order in the QCD coupling was made available.

First of all, we study the effect of the inclusion of QED corrections to perturbative evolution by comparing results obtained from our solution to the QED+QCD combined evolution equation as implemented in `FastKernel`, with those found when QED effects are switched off. For this first comparison, we assume that the photon PDF vanishes at a reference scale,  $\gamma(x, Q_0^2) = 0$  for  $Q_0^2 = 2 \text{ GeV}^2$ , and it is generated radiatively by evolution, and all other PDFs at the same scale are those from the Les Houches PDF benchmarks [39].

In Fig. 2 we plot the relative difference between PDFs evolved with and without QED corrections as a function of  $x$  at  $Q^2 = 10^3 \text{ GeV}^2$  for various PDFs, and the photon PDF which has been generated dynamically by perturbative evolution at three different scales. As expected, the QED corrections to all PDFs are small, below 1%, and concentrated at large  $x \gtrsim 0.1$ , while the dynamically generated photon PDF is very small at large  $x$  and then grows monotonically as  $x$  decreases. The correction to the up quark is larger than that to the down quark, because of larger absolute value of the former's electric charge.

We also compare our results for combined QED+QCD evolution to those obtained using the `partonevolution` code [38], version `v1.1.3`, bearing in mind that the two codes differ by terms of  $O(\alpha\alpha_s)$ . Indeed, the solution of Ref. [38] is based on the diagonalization of the full anomalous dimension matrix, rather than its factorization into QCD and QED components according to Eq. (2), although terms of  $O(\alpha\alpha_s)$  are also neglected. Our calculation should thus be equivalent up to subleading terms.

The comparison is shown in Fig. 2 for the photon PDF, and in Fig. 3 for the percentage differences of Fig. 2, here shown for two different PDF combinations at various scales. Excellent agreement is found, with differences between the two codes much smaller than the effect of QED corrections to the photon PDF or PDF evolution. We have also checked that the scale dependence obtained using our code is in good agreement with that of the MRST2004QED PDFs. These comparisons will be discussed in detail in Ref. [36].

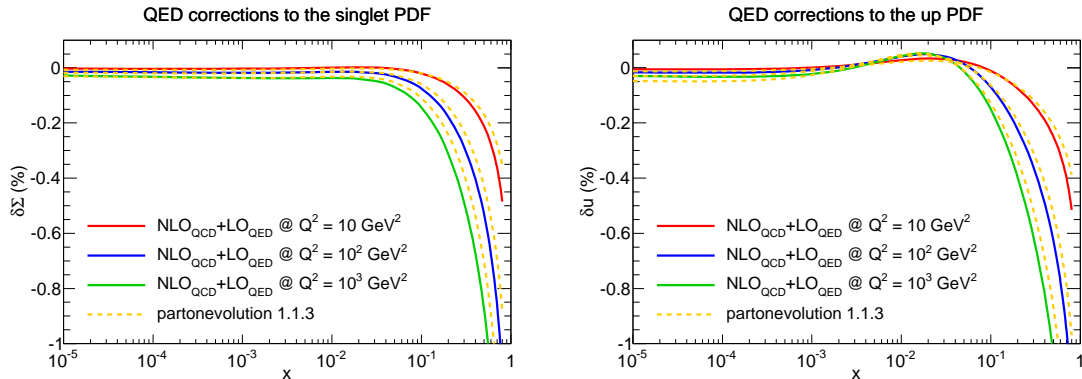


Figure 3: The relative differences of Fig. 2 for the singlet (left) and up (right) PDFs at  $Q^2 = 10, 10^2$  and  $10^3$  GeV<sup>2</sup>, computed using the NNPDF `FastKernel` implementation (solid curves) and the `partonevolution` code of Ref. [38, 40] (dashed curves).

## 2.2 Fitting PDFs with QED corrections

We now wish to obtain a first determination of the photon PDF from a fit to deep-inelastic data. We want to include QED corrections to DIS at LO, i.e., more accurately, the leading log level. This means that the splitting functions  $P^{\text{QED}}$  are computed to  $O(\alpha)$ , while all partonic cross sections (coefficient functions) are determined to lowest order in  $\alpha$ . Because the photon is electrically neutral, the photon deep-inelastic coefficient function only starts at  $O(\alpha^2)$ , while quark coefficient functions start at  $O(\alpha)$ . This means that at LO the photon coefficient function vanishes, and the photon only contributes to DIS through its mixing with quarks due to perturbative evolution. This is fully analogous to the role of the gluon in the standard LO QCD description of DIS: the gluon coefficient function only starts at  $O(\alpha_s)$  while the quark coefficient function starts at  $O(1)$ , so at LO the gluon only contributes to deep-inelastic scattering through its mixing with quarks upon perturbative evolution.

An important issue when including QED corrections is the choice of factorization scheme in the subtraction of QED collinear singularities [13, 41]. Different factorization schemes differ by next-to-leading log terms. Because our treatment of QED evolution is at the leading log level, our results do not depend on the choice of factorization scheme. This means that if our photon PDF is used in conjunction with a next-to-leading log computation of QED cross-sections, the latter can be taken in any (reasonable) factorization scheme. The difference in results found when changing the QED factorization scheme should be considered to be part of the theoretical uncertainty. However, in practice, in some schemes the perturbative expansion may show faster convergence (so, for example, next-to-leading log results are closer to leading-log ones in some schemes than others). We will indeed see in the next section that when DIS data are combined with Drell-Yan data it is advantageous to use the DIS factorization scheme, which is defined by requiring that the deep-inelastic structure function  $F_2$  is given to all orders by its leading-order expression [13, 41].

The starting point of our fit to DIS data including QED corrections is the NNPDF2.3 PDF determination, in terms of experimental data, theory settings and methodology. We



will perform fits at NLO and NNLO in QCD, for three different values of  $\alpha_s(M_Z) = 0.117, 0.118$  and  $0.119$ , all with LO QED evolution. Unless otherwise stated, in the following all results, tables, and plots will use the  $\alpha_s = 0.119$  PDF sets.

We add to the NNPDF default set of seven independent PDF combinations a new, independently parametrized PDF for the photon, in a completely analogous way to all other PDFs (see [25] and references therein), with a small modification related to positivity to be discussed below:

$$\gamma(x, Q_0^2) = (1-x)^{m_\gamma} x^{-n_\gamma} \text{NN}_\gamma(x), \quad (3)$$

where  $\text{NN}_\gamma(x)$  is a multi-layer feed-forward neural network with 2-5-3-1 architecture, with a total of 37 parameters to be determined by experimental data, and the prefactor is a preprocessing function used to speed up minimization, and on which the final result should not depend. The preprocessing function is parametrized by the exponents  $m_\gamma$  and  $n_\gamma$ , whose values are chosen at random for each replica, with uniform distribution in the range

$$1 \leq m_\gamma \leq 20, \quad -1.5 \leq n_\gamma \leq 1.5. \quad (4)$$

We have explicitly checked that the results are independent on the preprocessing range, by computing for each replica the effective small- and large- $x$  exponents [42], defined as

$$n_\gamma[\gamma(x, Q^2)] = \frac{\ln \gamma(x, Q^2)}{\ln \frac{1}{x}}, \quad m_\gamma[\gamma(x, Q^2)] = \frac{\ln \gamma(x, Q^2)}{\ln(1-x)}, \quad (5)$$

and verifying that the range of the effective exponents at small- and large- $x$  respectively is well within the range of variation of the preprocessing exponents, thus showing that the small- and large- $x$  behaviour of the best-fit PDFs is not constrained by the choice of preprocessing but rather determined by experimental data.

Parton distributions must satisfy positivity conditions which follow from the requirement that, even though PDFs are not directly physically observable, they must lead to positive-definite physical cross sections [43]. Leading-order PDFs are directly observable, and thus they must be positive-definite: indeed, they admit a probabilistic interpretation. Because we treat QED effects at LO, the photon PDF must be positive definite. This is achieved, as in the construction of the NNPDF2.1 LO PDF sets [44], by squaring the output of the neuron in the last (linear) layer of the neural network  $\text{NN}_\gamma(x)$ , so that  $\text{NN}_\gamma(x)$  is a positive semi-definite function.

Once QED evolution is switched on, isospin is no longer a good symmetry, and thus it can no longer be used to relate the PDFs of the proton and neutron. Because deuteron deep-inelastic scattering data are used in the fit, in principle this requires an independent parametrization for proton and neutron PDFs. Experimental data for the neutron PDFs would then no longer provide a useful constraint, and in particular they would no longer constrain the isospin triplet PDF. Whereas future PDF fits including substantially more LHC data might allow for an accurate PDF determination without using deuteron data, this does not seem to be possible at present.

There are two separate issues here: one, is the amount of isospin violation in the quark and gluon PDFs, and the second is the amount of isospin violation in the photon PDF. At the scale at which PDFs are parametrized, which is of the order of the nucleon mass, we expect isospin violating effects in the quark and gluon PDFs to be of the same order as that displayed in baryon spectroscopy, which is at the per mille level, much below the

Experiment	NLO		NNLO	
	QCD	QCD+QED	QCD	QCD+QED
Total	1.10	1.10	1.10	1.10
NMC-pd	0.88	0.87	0.88	0.88
NMC	1.68	1.70	1.67	1.69
SLAC	1.36	1.40	1.08	1.10
BCDMS	1.17	1.16	1.24	1.23
CHORUS	1.01	1.01	0.98	0.99
NTVDMN	0.54	0.54	0.56	0.54
HERAI-AV	1.01	1.01	1.04	1.03
FLH108	1.34	1.34	1.25	1.24
ZEUS-H2	1.26	1.25	1.24	1.25
ZEUS $F_2^c$	0.75	0.75	0.76	0.78
H1 $F_2^c$	1.55	1.50	1.41	1.39

Table 1: The  $\chi^2$  values per data point for individual experiments computed in the NNPDF2.3 DIS-only NLO and NNLO PDF sets, in the QCD-only fits compared to the results with combined QCD+QED evolution. All  $\chi^2$  values have been obtained using  $N_{\text{rep}}=100$  replicas with  $\alpha_s(M_Z) = 0.119$ . Normalization uncertainties have been included using the experimental definition of the covariance matrix, see App. A of Ref. [45], while in the actual fitting the  $t_0$  definition was used [46].

current PDF uncertainties (isospin violations of this order have been predicted, among others, on the basis of bag model estimates [47]). The second is the amount of isospin violation in the photon distribution itself: this could be somewhat larger (perhaps at the percent level), however any reasonable amount of isospin violation in the photon is way below the uncertainty on the photon PDF. Therefore, we will assume that no isospin violation is present at the initial scale.

Of course, even with isospin conserving PDFs at the starting scale, isospin violation is then generated by QED evolution: this is consistently accounted for when solving the evolution equations, by determining separate solutions for the proton and neutron so that at any scale  $Q \neq Q_0$ ,  $u^p(x, Q^2) \neq d^n(x, Q^2)$  and  $d^p(x, Q^2) \neq u^n(x, Q^2)$ . Because of the larger electric charge of the up quark, the dynamically generated photon PDF ends up being larger for the proton than it is for the neutron.

In Ref. [24] isospin violation was parametrized on the basis of model assumptions. We will compare our results for isospin violation to those of this reference in Sect. 3.2 below: we will see that while indeed the amount of isospin violation in the photon PDF from that reference is somewhat larger than our own, it is much smaller than the relevant uncertainty.

### 2.3 The photon PDF from DIS data

Using the standard NNPDF PDF parametrization supplemented with Eq. (3), we have performed two fits at NLO and NNLO to DIS data only, with the same settings used for NNPDF2.3, but with QED corrections in the PDF evolution now included, as discussed in the previous section.

The  $\chi^2$  for the fit to the total dataset and the individual DIS experiments are shown in Table 1, with and without QED corrections, and with QCD corrections included either at NLO or at NNLO. The  $\chi^2$  listed in the table use the so-called experimental definition

of the  $\chi^2$ , in which normalization uncertainties are included in the covariance matrix (see App. A of Ref. [45]): this definition is most suitable for benchmarking purposes, as it is independent of the fit results, but it is unsuitable for minimization as it would lead to biased fit results. It is clear that there is essentially no difference in fit quality between the QCD and QED+QCD fits. Indeed, a direct comparison of the PDFs obtained in the pairs of fits with and without QED corrections show that they differ very little.

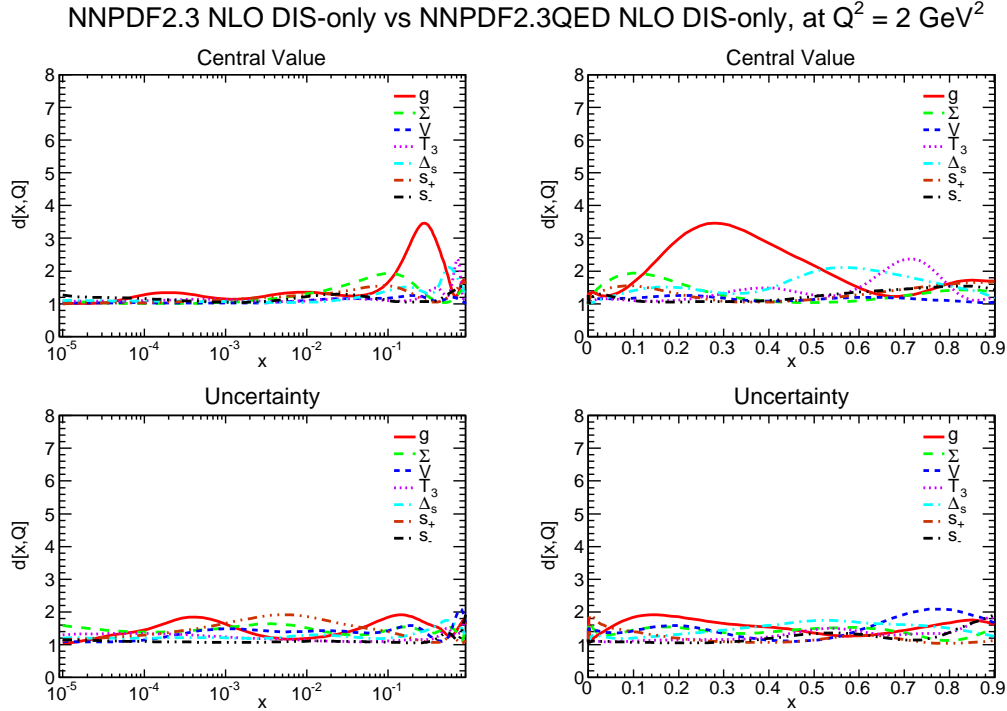


Figure 4: Distances between PDFs in the NNPDF2.3 NLO DIS-only fit and the fit including QED corrections, at the input scale of  $Q_0^2=2 \text{ GeV}^2$ . Distances between central values (top) and uncertainties (bottom) are shown, on a logarithmic (left) or linear (right) scale in  $x$ .

In order to assess this difference quantitatively, in Fig. 4 we plot the distance between central values and uncertainties of individual combinations of PDFs in the NLO QCD fit before and after the inclusion of QED corrections. We refer to Ref. [48] for a definition of the various combinations of PDFs and of the distance. Recall that for a set of  $N_{\text{rep}}$  PDF replicas,  $d \sim 1$  corresponds to PDFs extracted from the same underlying distribution (i.e. to statistically equivalent PDF sets), while  $d \sim \sqrt{N_{\text{rep}}}$  (so  $d \sim 10$  in our case) corresponds to PDFs extracted from distributions whose means or central values differ by one  $\sigma$ . The distances are shown in Fig. 4 for the NLO fit: it is clear that all PDFs but the gluon from the sets with and without QED corrections are statistically equivalent, while the gluon shows a change in the valence region of less than half  $\sigma$ . These results are unchanged when QCD is treated at NNLO order.

The fact that the inclusion of a photon PDF has a negligible impact on other PDFs can be also seen by determining the correlation between the photon and other PDFs. Results are shown in Fig 5. The correlation is negligible at the input scale, meaning that the particular shape of the photon in each replica has essentially no effect on the other PDFs

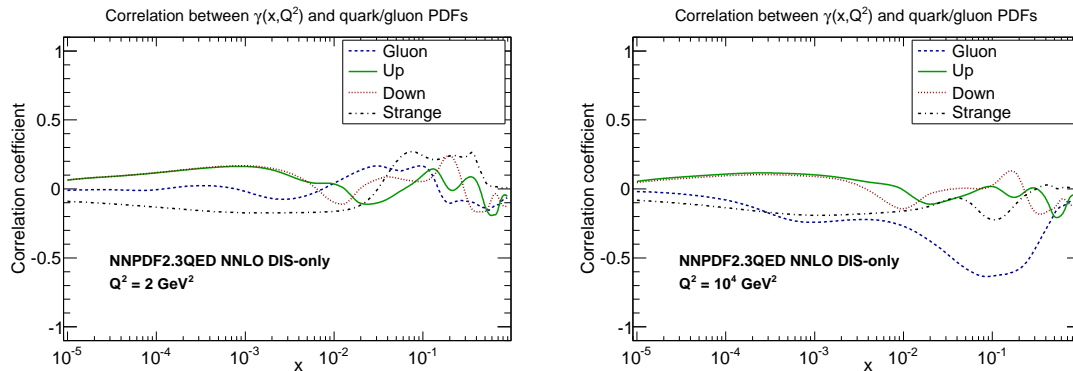


Figure 5: Correlation between the photon and other PDFs in the NNPDF2.3QED NLO DIS-only fit, shown as a function of  $x$  at the input scale  $Q_0^2 = 2 \text{ GeV}^2$  (left) and at  $Q^2 = 10^4 \text{ GeV}^2$ .

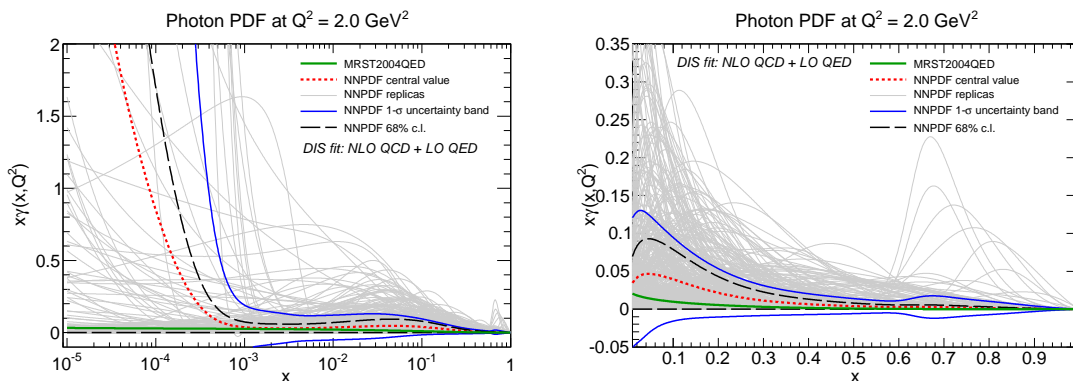


Figure 6: The photon PDF determined from the NNPDF2.3QED NLO DIS-only fit, in a linear (left plot) and logarithmic (right plot) scales,  $N_{\text{rep}} = 500$ . We show the central value (mean), the individual replicas and the PDF uncertainty band defined as a one  $\sigma$  interval and as a symmetric 68% confidence level centered at the mean. The MRST2004QED photon PDF is also shown.

of that replica. In particular, this correlation is much smaller than that which arises at a higher scale (also shown in Fig. 5), due to the mixing of PDFs with the photon induced by PDF evolution.

Hence, at the initial scale  $Q_0^2 = 2 \text{ GeV}^2$  the sets with and without QED corrections differ mainly because of the presence of a photon PDF in the latter. The photon PDF determined in the NLO fit is shown in Fig. 6 at  $Q_0^2 = 2 \text{ GeV}^2$ : the individual replicas, the mean value, the one- $\sigma$  range and the 68% confidence interval are all shown. The MRST2004QED photon PDF is also shown. It is clear that positivity imposes a strong constraint on the photon PDF, which is only very loosely constrained by DIS data. As a consequence, the probability distribution of replicas is very asymmetric: some replicas may have large positive values of  $\gamma(x, Q^2)$ , but positivity always ensures that no replica goes below zero. It follows that the usual gaussian assumptions cannot be made, and in particular there is a certain latitude in how to define the uncertainty. Here and in the remainder of this paper we will always define central values as the mean of the distribution, and uncertainties as symmetric 68% confidence levels centered at the mean, namely, as

the symmetric interval centered at the mean such that 68% of the replicas falls within it. All uncertainty bands will be determined in this way, unless otherwise stated. Because of the accumulation of replicas just above zero, the lower edge of the uncertainty band on the photon PDF at the initial scale turns out to be very close to zero. Again, results are essentially unchanged when the fit is done using NNLO QCD theory.

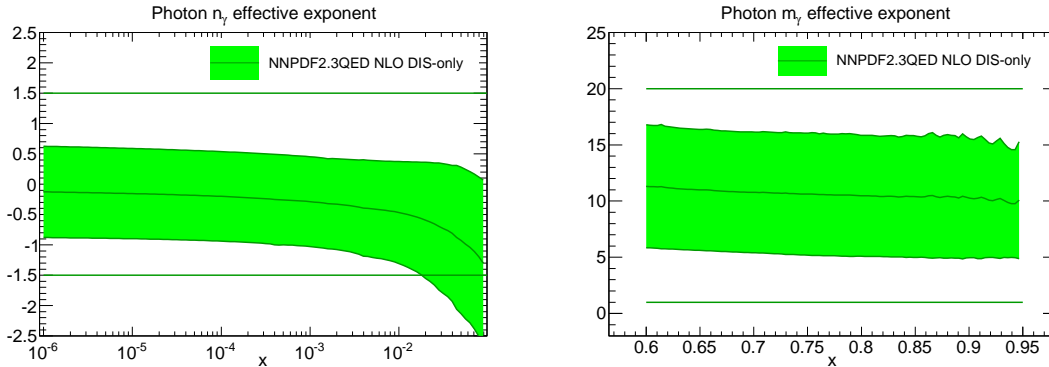


Figure 7: One- $\sigma$  range for the effective exponents Eq. (5) for the photon PDF, compared to the range of variation of the preprocessing exponents Eq. (4) (shown as horizontal lines).

As discussed in Sect. 2.2, we have determined the effective exponents Eq. (5) for the photon PDF, and compared them to the range of variation of the preprocessing exponents Eq. (4). Given the very loose constraints that the data impose on the photon PDF, it is especially important to make sure that preprocessing imposes no bias. The comparison is shown in Fig. 7: it is clear that the effective exponents are well within the range chosen for the preprocessing exponents, so that no bias is being introduced.

The photon PDF at the initial scale shown in Fig. 6 is essentially compatible with zero, and it remains small even at the top of its uncertainty band; it is consistent with the MRST2004QED photon PDF within its large uncertainty band.

The momentum fraction carried by the photon is accordingly small: it is shown as a function of scale in Fig. 8 for the NLO fit; results at NNLO are very similar. At the input scale  $Q_0^2 = 2 \text{ GeV}^2$  we find

$$\int_0^1 x\gamma(x, Q_0^2) = (1.26 \pm 1.26) \% , \quad (6)$$

The symmetric 68% confidence level uncertainty of Eq. (6) turns out to be quite close to the standard deviation  $\sigma = 1.36\%$ . Hence, even at the top of its uncertainty range the photon momentum fraction hardly exceeds 2%, and it is compatible with zero to one  $\sigma$ . The momentum fraction carried by the the MRST2004QED photon (also shown in Fig. 8) is well below 1%, and thus compatible with our own within uncertainties

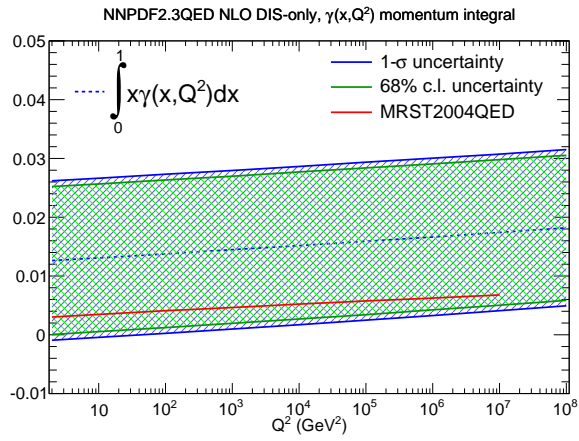


Figure 8: The momentum fraction carried by the photon PDF in the NLO fit as a function of scale. The MRST2004QED result is also shown.

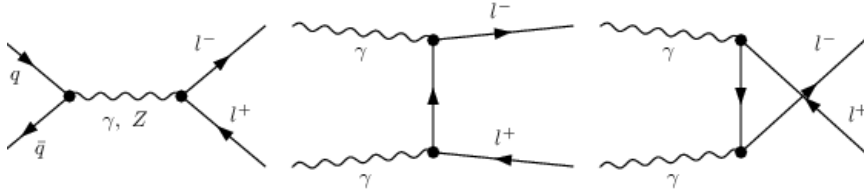


Figure 9: Feynman diagrams for the Born-level partonic subprocesses which contribute to the production of dilepton pairs in hadronic collisions.

### 3 The photon PDF from $W$ and $Z$ production at the LHC

The photon PDF  $\gamma(x, Q^2)$  determined in the previous section from a fit to DIS data is affected by very large uncertainties. This suggests that its impact on predictions for hadron collider processes to which the photon PDF contributes already at leading order could be substantial, and thus, conversely, that data on such processes might provide further constraints. In this section we use the simplest of such processes, namely, electroweak gauge boson production, to constrain the photon PDF.

At hadron colliders, the dilepton production process receives contributions at Born level both from quark-initiated neutral current  $Z/\gamma^*$  exchange and from photon-initiated diagrams, see Fig. 9, and thus the contributions from  $\gamma(x, Q^2)$  must be included even in a pure leading-order treatment of QED effects. Photon-initiated contributions to dilepton production at hadron colliders were recently emphasized in Ref. [13], where  $O(\alpha)$  radiative corrections to this process [3, 5–13] were reassessed, and also kinematic cuts to enhance the sensitivity to  $\gamma(x, Q^2)$  were suggested.

Beyond the Born approximation, radiative corrections to the neutral-current process, as well as the charged-current process, which starts at  $O(\alpha)$  (see Fig. 10 for some representative Feynman diagrams) may be comparable in size to the Born level contribution, because the suppression due to the extra power of  $\alpha$  might be compensated by the enhancement arising from the larger size of the quark-photon parton luminosity in comparison to the photon-photon luminosity. However, a full inclusion of  $O(\alpha)$  corrections would require solving evolution equations to NLO in the QED and mixed QED+QCD terms, so it is beyond the scope of this work; we will nevertheless discuss an approximate inclusion of such corrections which, while not allowing us to claim more than LO accuracy in QED, should ensure that NLO QED corrections are not unnaturally large.

We use neutral and charged-current Drell-Yan production data from the LHC to further constrain the photon PDF, thereby arriving at our final NNPDF2.3QED PDF sets. As discussed in the introduction, we do this by combining the photon PDF from NNPDF2.3 DIS-only set discussed in the previous section with the standard NNPDF2.3 PDF set, and then using gauge boson production data to reweight the result. We discuss first this two-step fitting procedure, and then the ensuing NNPDF2.3QED PDF set and its features.

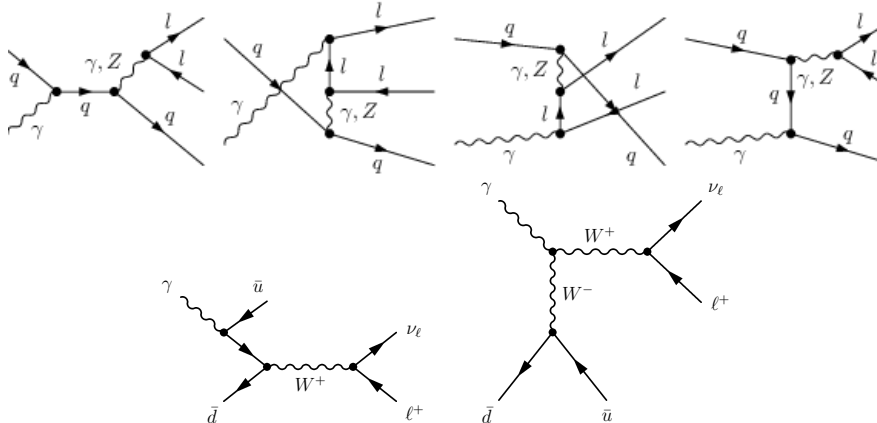


Figure 10: Some Feynman diagrams for  $O(\alpha)$  photon-initiated partonic subprocesses which contribute to neutral current (top row) and charged current (bottom row) dilepton pair production in hadronic collisions.

### 3.1 The prior NNPDF2.3QED and its reweighting

As a first step towards the determination of a PDF set with inclusion of QED corrections, we would like to use the photon PDF determined in the previous section from a fit to DIS data in conjunction with PDFs which retain all the information provided by the full NNPDF2.3 data set, which, on top of DIS, includes Drell-Yan and jet production data from the Tevatron and the LHC.

We have seen in the previous section that all PDFs determined including QED corrections are statistically equivalent to their standard counterparts determined when QED corrections are not included, with the only exception of the gluon, which undergoes a change by less than half  $\sigma$  in a limited kinematic region. Furthermore, the photon in each PDF replica is essentially uncorrelated to the shape of other PDFs which are input to perturbative evolution, the only significant correlation being due to the mixing induced by the evolution itself. We can therefore simply combine the photon PDF obtained from the DIS fit of the previous section with the standard NNPDF2.3 PDFs at the starting scale  $Q_0^2$ . This procedure entails a certain loss of accuracy, which in particular appears as a violation of the momentum sum rule of the order of the momentum fraction carried by the photon at the initial scale Eq. (6), namely of order 1%. This is the accuracy to which the momentum sum rule would be verified if it were not imposed as a constraint in the fit [44].

The information contained in LHC Drell-Yan production data is included in the fit through the Bayesian reweighting method presented in Ref. [30,31]. This method allows for the inclusion of new data without having to perform a full refit, by using Bayes' theorem to modify the prior probability distribution of PDF replicas in order to account for the information contained in the new data. The ensuing replica set contains an amount of information, and thus allows for the computation of observables with an accuracy, that corresponds to an effective number of replicas  $N_{\text{eff}}$ , which may be determined from the Shannon entropy of the reweighted set.

In our case, the new data only constrain significantly the photon PDF, hence we need



Dataset	Observable	Ref.	$N_{\text{dat}}$	$[\eta_{\text{min}}, \eta_{\text{max}}]$	$M_{\text{ll}}^{\text{min}}, M_{\text{ll}}^{\text{max}}$
LHCb $\gamma^*/Z$ Low Mass	$d\sigma(Z)/dM_{\text{ll}}$	[49]	9	[2,4.5]	[5,120] GeV
ATLAS $W, Z$	$d\sigma(W^\pm, Z)/d\eta$	[50]	30	[-2.5,2.5]	[60,120] GeV
ATLAS $\gamma^*/Z$ High Mass	$d\sigma(Z)/dM_{\text{ll}}$	[51]	13	[-2.5,2.5]	[116,1500] GeV

Table 2: Kinematical coverage of the three LHC datasets used to determine the photon PDF.

to guarantee that good accuracy is obtained by starting with a large number of photon PDF replicas. The initial prior set is thus obtained combining 500 photon PDF replicas with a standard set of 100 NNPDF2.3 replicas. In practice, this is done by simply producing five copies of the NNPDF2.3 100 replica set, and combining each of them at random with one of the 500 photon PDF replicas obtained from the QED fit to DIS data discussed in the previous section. The procedure is performed at NLO and NNLO, in each case combining the photon PDF from the combined QED+QCD fit to DIS data with the other PDFs from the corresponding standard NNPDF2.3 set. Furthermore, the procedure is repeated for three different values of  $\alpha_s = 0.117, 0.118, 0.119$ . We find no dependence of the photon PDF on the value of  $\alpha_s$ , though there are minor differences between the photon determined using NLO or NNLO QCD theory in the DIS fit.

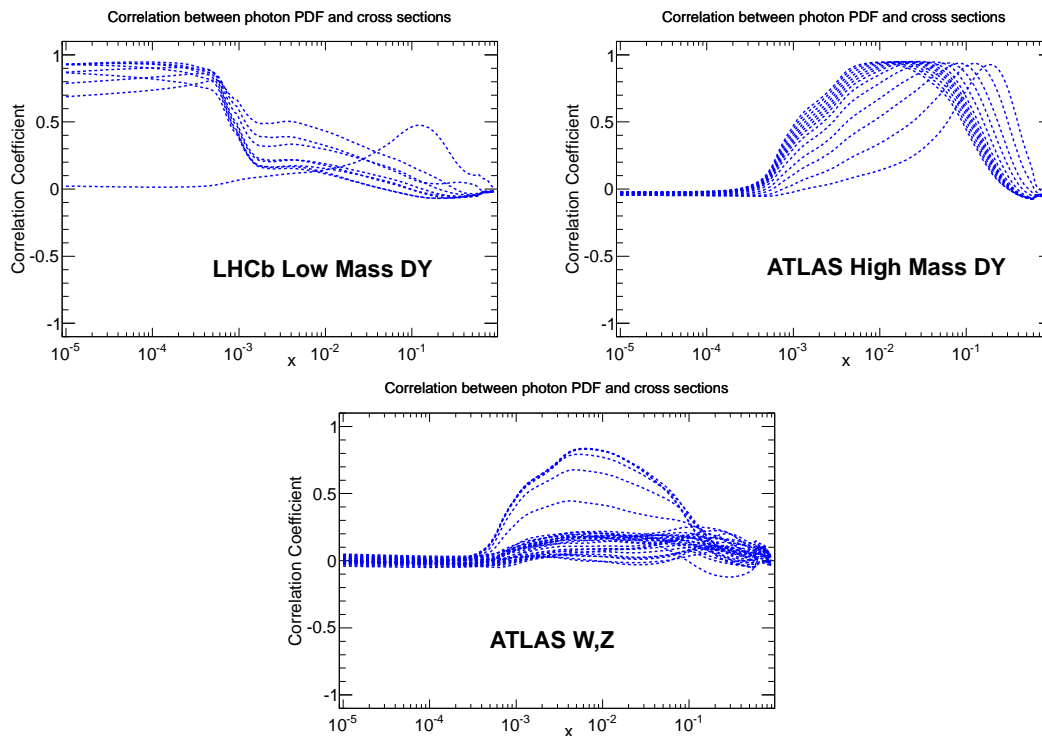


Figure 11: Correlation between the photon PDF and the LHC data of Tab. 2, shown as function of  $x$  for  $Q^2 = 10^4 \text{ GeV}^2$ . Each curve corresponds to an individual data bin.

In each case, the set of  $N_{\text{rep}} = 500$  replicas is then evolved to all scales using combined QED+QCD evolution. Note that this in particular implies that no further violation of the momentum sum rule is introduced on top of that which was present at the initial scale,

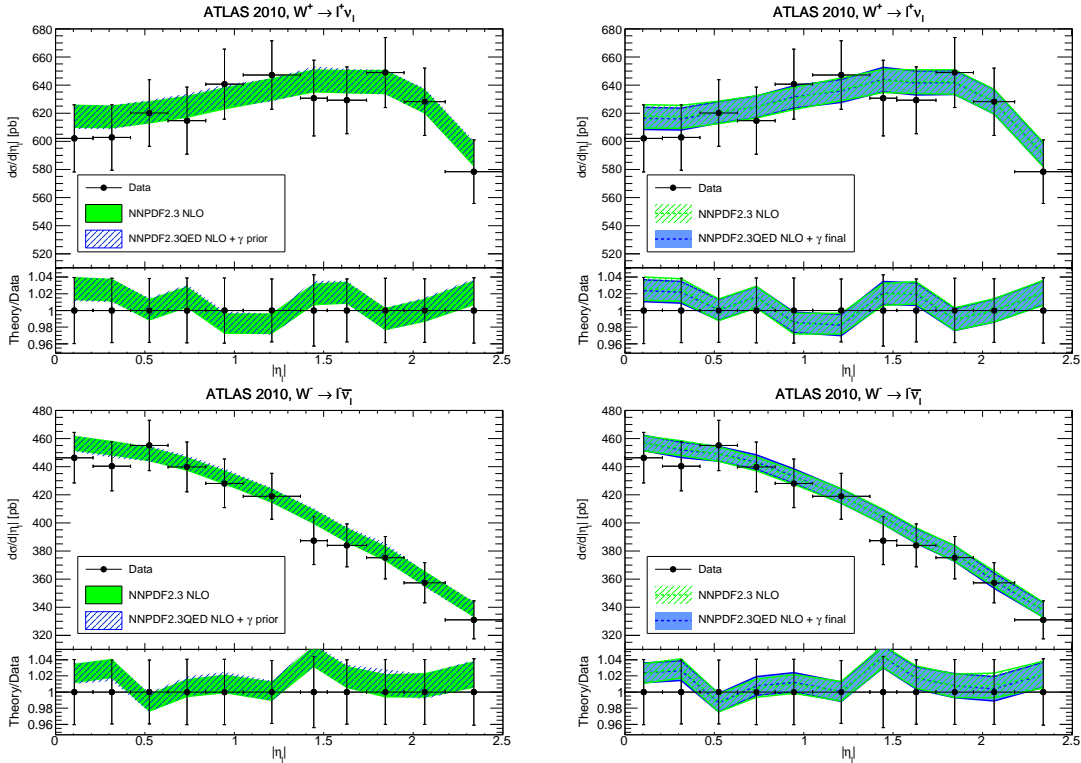


Figure 12: Comparison of the ATLAS  $W$  production data with NLO theoretical predictions obtained using PDFs before (left) and after (right) reweighting with the data of Tab. 2. In all plots we also show for comparison results obtained using the default NNPDF2.3 PDF set, with all QED corrections switched off. From top to bottom:  $W^+$  and  $W^-$ . Error bands on the theoretical prediction correspond to one  $\sigma$  uncertainties. Experimental error bars give the total combined statistical and systematic uncertainty.

up to approximations introduced when solving the evolution equations.

Reweightings is performed using the following LHC datasets:

- LHCb low-mass  $Z/\gamma^*$  Drell-Yan production from the 2010 run [49]
- ATLAS inclusive  $W$  and  $Z$  production data from the 2010 run [50]
- ATLAS high-mass  $Z/\gamma^*$  Drell-Yan production from the 2011 run [51],

whose kinematic coverage is summarized in Table 2. Using data with three different mass ranges for the dilepton pairs, below, at, and above the  $W$  and  $Z$  mass, guarantees that both the low  $x$  (from low mass) and high  $x$  (from high mass) regions are covered.

For all the ATLAS data the experimental covariance matrix is available, hence the  $\chi^2$  may be computed fully accounting for correlated systematics. This is not the case for LHCb: hence, the low-mass data are treated adding statistical and systematic errors in quadrature, and only including normalization errors in the covariance matrix. We have checked that if reweighting is performed using the diagonal covariance matrix, statistically indistinguishable results are obtained. This means that within the large uncertainty of the photon PDF, and due to the small impact of QED corrections on the quark and gluon

PDFs, the lack of information on correlations for the LHCb experiment is immaterial. However, this implies that  $\chi^2$  values quoted for LHCb should only be taken as indicative. Unfortunately, the CMS off-peak Drell-Yan data [52] is not yet publicly available, and thus could not be used in the present analysis.

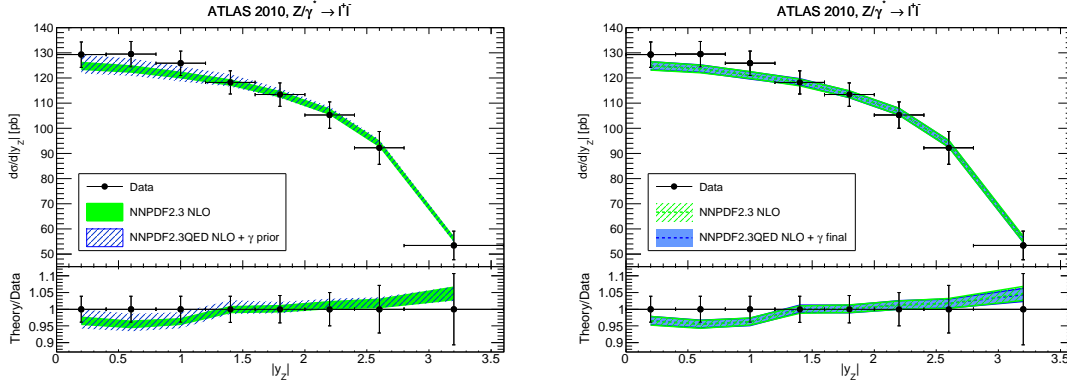


Figure 13: Same as Fig. 12, but for the neutral current data.

The range of  $x$  for the photon PDF which is affected by each of the datasets of Table 2 can be determined quantitatively by computing the correlation coefficient (see [53] and Sect. 4.2 of Ref. [54]) between a given observable and the PDFs. The correlation coefficients computed using the NNPDF2.3QED NLO prior set are shown in Fig. 11 for each bin in the experiments in Table 2. It is clear that the LHC data guarantee a good kinematic coverage for all  $10^{-5} \lesssim x \lesssim 0.1$ . The correlation is weaker for real  $W$  and  $Z$  production data, where the  $s$ -channel quark contribution dominates as the propagator goes on shell. The high-mass (low-mass) Drell-Yan data is thus essential to pin down  $\gamma(x, Q^2)$  at large (small) Bjorken- $x$ , where uncertainties are the largest. Indeed, a preliminary determination of the photon distribution [55], which did not use the LHCb data, had significantly larger uncertainties at small  $x$ , consistently with the expectations based on the correlation plot of Fig. 11.

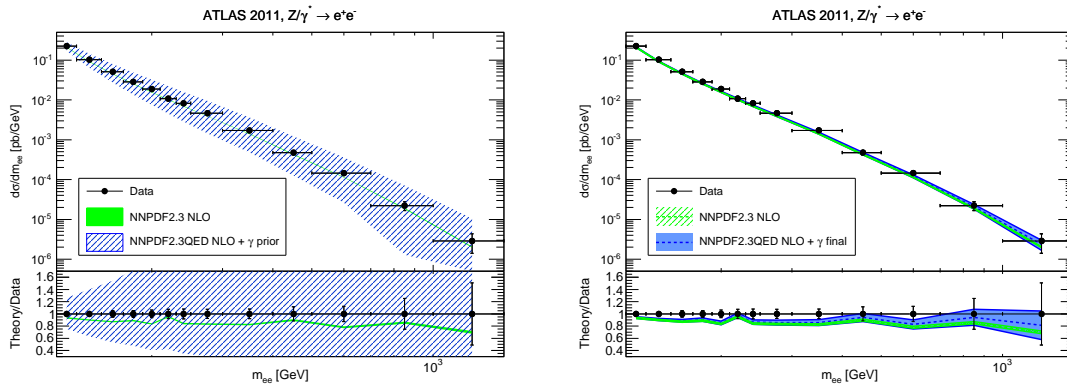


Figure 14: Same as Fig. 12, but for the ATLAS high-mass neutral-current data.

Theoretical predictions for the datasets in Table 2 have been computed at NLO and NNLO in QCD using DYNLLO [56], supplemented with Born-level and  $O(\alpha)$  QED correc-

tions using **HORACE** [11, 12]. Results from **DYNNLO** and **HORACE** have been combined additively, avoiding double counting, in order to obtain a consistent combined QCD+QED theory prediction. The additive combination of QED and QCD corrections avoids introducing  $O(\alpha\alpha_s)$  terms, which are beyond the accuracy of our calculation. In the **DYNNLO** calculation, the renormalization and factorization scale have been set to the invariant mass of the dilepton pair in each bin. The **HORACE** default settings, with the renormalization and factorization set to the mass of the gauge boson, have been used for the ATLAS high-mass data, but we have also checked that for this data the choice is immaterial, in that the LO results obtained using **DYNNLO** and **HORACE** with the respective scale settings agree with each other.

For the LHCb low-mass data we have used a modified version of **HORACE** in which the scale choice is the same as in **DYNNLO**, since for these low scale data the choice of renormalization and factorization scale does make a significant difference. Note that the smallest mass values reached by these data correspond to momentum fractions  $x \sim 10^{-3}$  in the central rapidity regions, for which, at the scale of the data, fixed order (unresummed) results are expected to be adequate (see Ref. [57], in particular Fig. 1). Indeed we shall see that our results are perturbatively stable in that the photon PDF at NLO and NNLO is very similar for all  $x$  (see Figs.16-17 below).

The same selection and kinematical cuts as in the corresponding experimental analysis has been adopted: in particular, the same requirements concerning lepton-photon final state recombination and the treatment of final state QED radiation have been implemented in the **HORACE** computations.

It should be noticed that, whereas the LHCb and ATLAS high-mass data are only being included now in the fit, the  $W$  and  $Z$  production data were already included in the original NNPDF2.3 PDF determination (where they turned out to have a moderate impact). Therefore, in principle a modified version of NNPDF2.3 in which these data are removed from the fit should have been used as a prior. In practice, however, this would make very little difference. We have verified that the inclusion of QED evolution affects minimally the prediction for this data, where differences are at the same level of the Monte Carlo integration uncertainty, as can also be seen from Fig. 2, recalling (see Fig. 11) that the main impact of this data is in the  $x \sim 0.01$  region. This means that the contributions to this process in the reweighting and in the original NNPDF2.3 fit in practice only differ because of the inclusion of the photon contribution. Furthermore, we have explicitly verified that if the ATLAS  $W$  and  $Z$  production data are excluded from the fit, the photon is systematically modified by a small but non-negligible amount (less than half  $\sigma$  at most) in the region  $x \sim 10^{-3}$  where these data are expected to carry information (see Fig. 11), while all other PDFs are essentially unaffected.

Whereas our computation is only accurate to leading order in QED, we did include  $O(\alpha)$  corrections to the electroweak gauge boson production process through **HORACE**, with the aim of avoiding unnaturally large NLO QED corrections. This raises several issues which we now discuss in turn.

As pointed out in Refs. [13, 41], usage of the leading-order expressions in QED for the DIS coefficient functions can be viewed as the choice of the DIS factorization scheme, in which deep-inelastic coefficient functions are taken to coincide to all orders with their leading-order expression, with higher order corrections factorized into the PDFs. Therefore, use of the DIS scheme for the QED corrections to the Drell-Yan process ensures

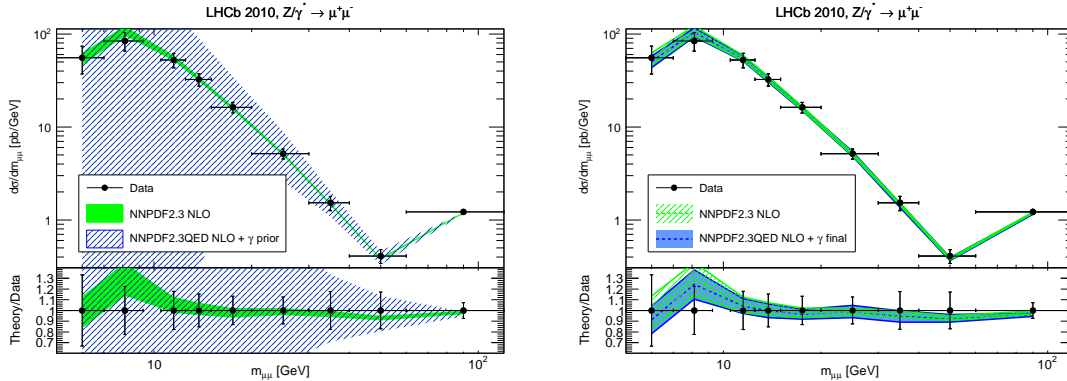


Figure 15: Same as Fig. 12, but for the LHCb low-mass neutral current data.

that predictions for Drell-Yan obtained with PDFs determined using DIS data and LO QED are actually accurate up to NLO, modulo any NLO corrections from QED evolution. Therefore, we have used the DIS-scheme expressions for NLO corrections to Drell-Yan as implemented in `HORACE`. Of course, in practice, there will be NLO QED evolution effects, even though there is a certain overlap between the kinematic region of the HERA DIS data and that of the LHC Drell-Yan data, so we cannot claim NLO QED accuracy. However we expect this procedure to lead to greater stability of our results upon the inclusion of NLO QED corrections.

Radiative corrections related to final-state QED radiation have already been subtracted from the ATLAS data, but not from the LHCb data. Therefore, for ATLAS we have only included photon-induced processes in the `HORACE` runs, while for LHCb we have also included explicit  $O(\alpha)$  contributions from final-state QED radiation. Electroweak corrections, which are not subtracted from any of the data and which are not included in our calculation, could be potentially relevant in the high-mass region [13]. However, in practice they are always much smaller than the statistical uncertainty on the ATLAS data.

Finally, to NLO in QED the scheme used in defining electroweak couplings should be specified. The `DYNNLO` code uses the so-called  $G_\mu$  scheme for the electroweak couplings, while `HORACE` also uses the  $G_\mu$  scheme for charged-current production, but the improved Born approximation for neutral-current production. We have verified the differences in predictions between the two scheme are negligible in comparison to the statistical uncertainties of the Monte Carlo integrations.

### 3.2 The NNPDF2.3QED set

The NNPDF2.3QED PDF set is obtained by performing a reweighting of the prior  $N_{\text{rep}} = 500$  replica set with the data of Table 2. The procedure is performed at NLO and NNLO in QCD, with three different values of  $\alpha_s$  in each case. The theoretical prediction used for reweighting is computed as discussed in the previous section, and the  $\chi^2$  used for reweighting is then determined from its comparison to the data, using the fully correlated systematics for the two ATLAS experiments, for which the covariance matrix is available, but adding statistical and systematic errors in quadrature for LHCb, for which information

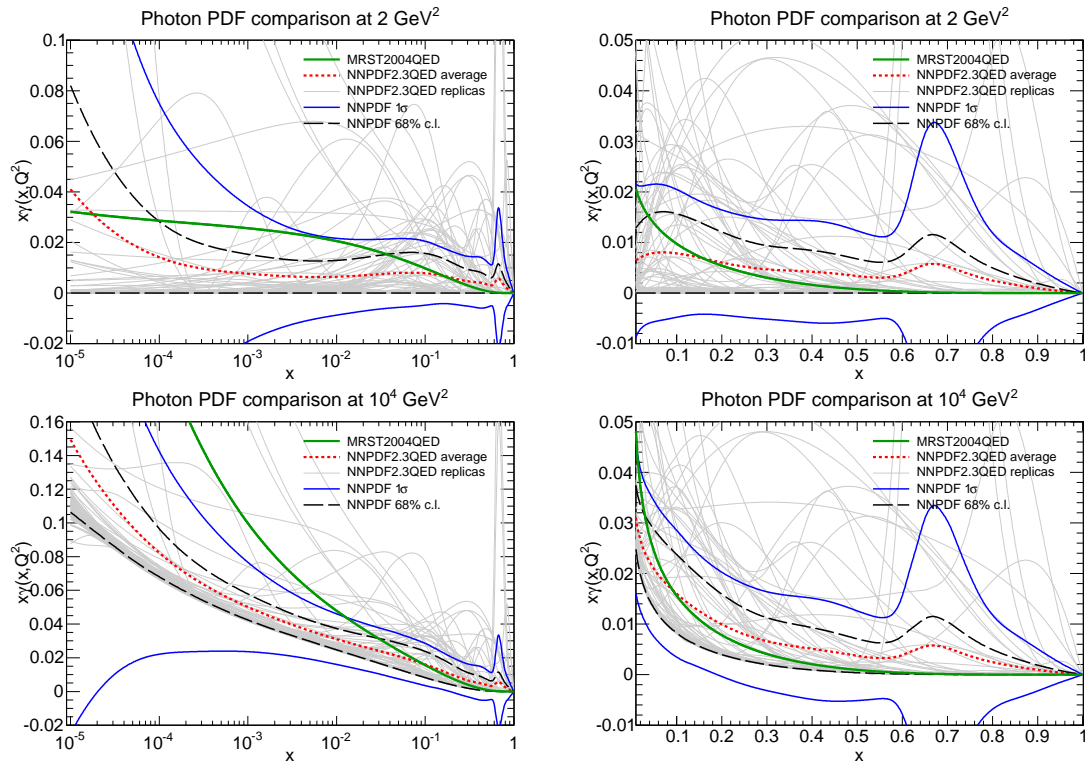


Figure 16: The NNPDF2.3QED NLO photon PDF at  $Q^2 = 2 \text{ GeV}^2$  and  $Q^2 = 10^4 \text{ GeV}^2$  plotted vs.  $x$  on a log (left) or linear (right) scale. The 100 replicas are shown, along with the mean, the one- $\sigma$ , and the 68% confidence level ranges. The MRST2004QED photon PDF is also shown for comparison.

on correlations is not available. The ensuing weighted set of replicas is then unweighted [31] to obtain a standard set of  $N_{\text{rep}} = 100$  replicas.

The parameters of the reweighting are collected in Table 3: we show the  $\chi^2$  (divided by the number of data points) for the data of Table 2 before and after reweighting, the effective number of replicas after reweighting, and the mean value of  $\alpha$ , the parameter which measures the consistency of the data which are used for reweighting with those included in the prior set, by providing the factor by which the uncertainty on the new data must be rescaled in order of the two sets to be consistent (so  $\alpha \sim 1$  means consistent data). Values are given for reweighting performed using each individual dataset, and the three datasets combined. All  $\chi^2$  values are computed using the experimental definition of the covariance matrix as in Table 1; the same form of the covariance matrix has also been used for reweighting for simplicity, as this choice is immaterial as discussed above.

In all cases the final effective number replicas turns out to be  $N_{\text{eff}} > 100$ , thereby guaranteeing the accuracy of the final unweighted set. All sets show good compatibility with the prior datasets. The final  $\chi^2$  values show that the reweighted set provides an essentially perfect fit to the data; the low values for LHCb are a consequence of the fact that for this experiment the correlated systematics is not available so statistical and systematic errors are added in quadrature. Before reweighting the  $\chi^2$  of individual replicas shows wide fluctuations: indeed, its average and variance over the starting replica sample

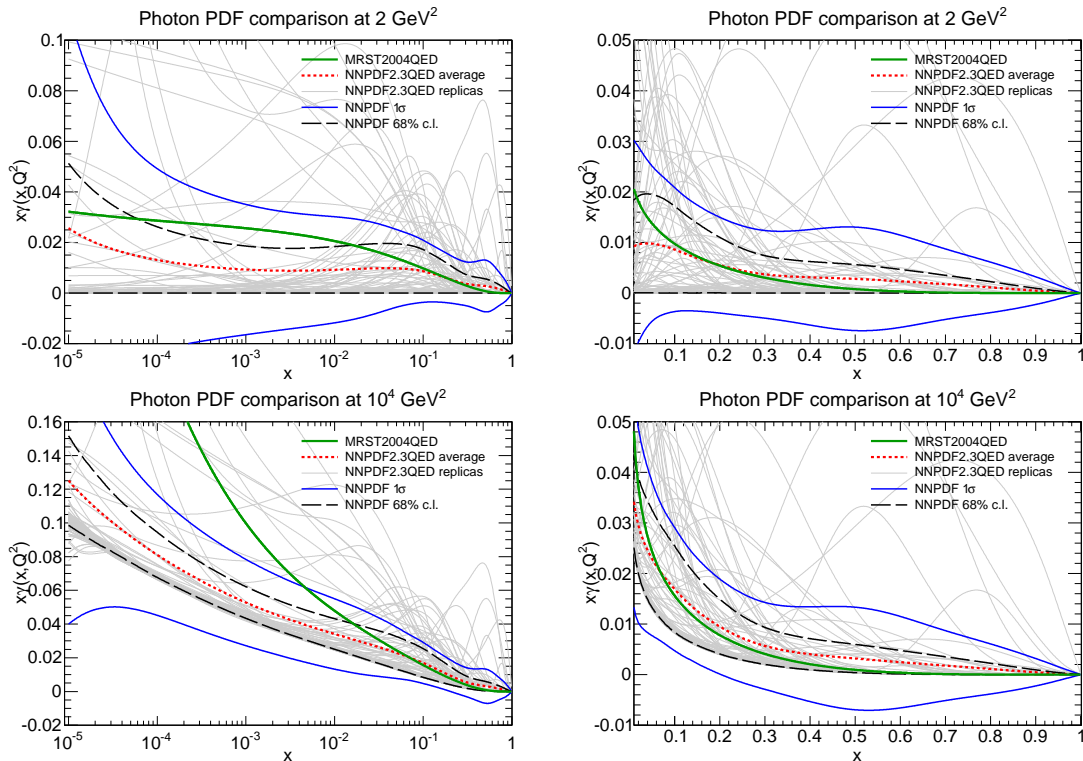


Figure 17: Same as 16 for the NNPDF2.3QED NNLO PDF set.

are given by  $\langle \chi^2 \rangle = 25.6 \pm 164.4$ . After reweighting the value becomes  $\langle \chi^2 \rangle = 1.117 \pm 0.098$ , thus showing that the  $\chi^2$  of individual replicas has become on average almost as good as that of the central reweighted prediction.

A first assessment of the impact of the photon-induced corrections and their effect on the photon PDF can be obtained by comparing the data to the theoretical prediction obtained using pure QCD theory and the default NNPDF2.3 set, QCD+QED with the prior photon PDF, and QED+QCD with the final NNPDF2.3QED set. The comparison is shown in Figs. 12-15 for the NLO sets (the NNLO results are very similar): in the left plots we show the QED+QCD prediction obtained using the prior PDF set, and in the right plots the prediction obtained using the final reweighted sets, compared in both cases to the pure QCD prediction obtained using DYNL0 and the NNPDF2.3 set. At the  $W, Z$  peak, the impact of QED corrections is quite small, though, in the case of neutral current production, to which the photon-photon process contributes at Born level, when the prior photon PDF is used one can see the widening of the uncertainty band due to the large uncertainty of the photon PDF of Fig. 6. At low or high mass, as one moves away from the peak, the large uncertainty on the prior photon PDF induces an increasingly large uncertainty on the theoretical prediction, substantially larger than the data uncertainty. This means that these data do constrain the photon PDF and indeed after reweighting the uncertainty is substantially reduced.

The final NNPDF2.3QED photon PDF obtained in the NLO and NNLO fits is respectively shown at  $Q_0^2 = 2 \text{ GeV}^2$  in Fig. 16 and Fig. 17. We display individual replicas,

NLO				
	LHCtot	ATLAS $W, Z$	ATLAS high mass DY	LHCb low-mass DY
$\chi_{\text{in}}^2$	2.02	1.20	3.78	2.20
$\chi_{\text{rw}}^2$	1.00	1.15	1.01	0.29
$N_{\text{eff}}$	287	364	326	267
$\langle\alpha\rangle$	1.41	1.24	1.53	0.89

NNLO				
	LHCtot	ATLAS $W, Z$	ATLAS high mass DY	LHCb low-mass DY
$\chi_{\text{in}}^2$	2.01	1.37	3.44	2.06
$\chi_{\text{rw}}^2$	1.08	1.21	1.00	0.66
$N_{\text{eff}}$	197	297	330	363
$\langle\alpha\rangle$	1.48	1.33	1.52	1.20

Table 3: Reweighting parameters in the construction of the final NNPDF2.3 sets. All  $\chi^2$  values are defined as in Tab. 1.

	NNPDF2.3QED NLO	NNPDF2.3QED NNLO	MRST2004QED
$\gamma; Q^2 = 2 \text{ GeV}^2$	$(0.42 \pm 0.42)\%$	$(0.34 \pm 0.34)\%$	0.30%
$\gamma; Q^2 = 10^4 \text{ GeV}^2$	$(0.68 \pm 0.42)\%$	$(0.61 \pm 0.34)\%$	0.52%
total; $Q^2 = 2 \text{ GeV}^2$	$(100.43 \pm 0.44)\%$	$(100.32 \pm 0.34)\%$	99.95%
total; $Q^2 = 10^4 \text{ GeV}^2$	$(100.38 \pm 0.43)\%$	$(100.29 \pm 0.36)\%$	99.92%

Table 4: Momentum fractions (in percentage) carried by the photon PDF (upper two rows) and by the sum of all partons in the proton (lower two rows) in the NNPDF2.3QED NLO, NNLO and MRST2004QED PDF sets at two different scales

the central (mean) photon, and the one- $\sigma$  and 68% confidence level ranges, as well as the MRST2004QED result. The improvement in accuracy in comparison to the prior PDF of Fig. 6 is apparent, especially at small and at large  $x$ . Note also that, especially at large  $x$ , where the experimental information remains scarce (recall Fig. 11), the positivity bound still plays an important role in constraining the photon PDF. Indeed, at the starting scale  $Q_0$  the lower edge of the uncertainty band (determined as discussed in Sect. 2) is again very close to the positivity constraint, and consequently, even after having used the LHC data, the probability distribution of the photon PDF is significantly asymmetric, departing substantially from Gaussian. This should be kept in mind in phenomenological applications, in particular when computing uncertainties.

In Table 4 we show the momentum fraction carried by the photon PDF in NNPDF2.3QED at NLO and NNLO, both at a low and high scale: it is about half of a percent, compatible with zero within uncertainties, and mildly dependent on scale. The MRST2004QED values, also shown, are consistent within uncertainties. Note that the standard deviation would be almost twice the 68% confidence level interval given in the table. We also give the total momentum, which deviates from unity because of the slightly inconsistent procedure



### NNPDF2.3 NLO vs NNPDF2.3QED NLO, at $Q^2 = 2 \text{ GeV}^2$

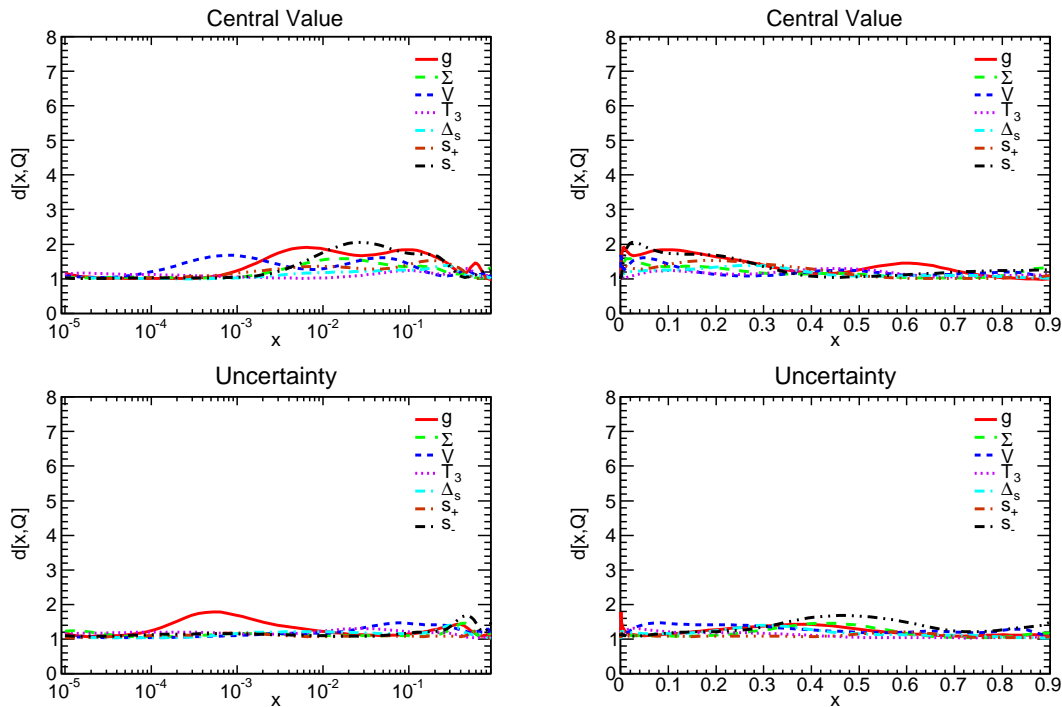


Figure 18: Distances between PDFs in the NNPDF2.3 and the NNPDF2.3QED NLO sets, at the input scale of  $Q_0^2=2 \text{ GeV}^2$ . Distances between central values (top) and uncertainties (bottom) are shown, on a logarithmic (left) and linear (right) scale in  $x$ .

that we have followed in constructing the prior set, by combining the photon from a fit to DIS data with the other PDFs from the global NNPDF2.3 fit as discussed in Sect. 3.1 above. We also see that the total momentum fraction is not quite scale independent, because of the approximation introduced when neglecting terms of  $O(\alpha\alpha_s)$  in the solution of the combined QED+QCD evolution equations. Both effects are well below the 1% level.

All other PDFs at the initial scale  $Q_0$  are left unaffected by the reweighting. This can be seen by computing the distances between PDFs in the starting NNPDF2.3 set and in the final NNPDF2.3QED set; they are displayed in Fig. 18, at the scale  $Q_0^2 = 2 \text{ GeV}^2$  at which PDFs are parametrized: it is apparent that the distances are compatible with statistically equivalent PDFs. It is interesting to repeat the same comparison at  $Q^2 = 10^4 \text{ GeV}^2$  (Fig. 19): in this case, statistically significant differences start appearing, as a consequence of the fact that the statistically equivalent starting PDFs in the two sets are then evolved respectively with and without QED corrections. However, the differences are below the one- $\sigma$  level (and concentrated at large  $x$ ), consistent with the conclusion that the new data are compatible with those used for the determination of the NNPDF2.3 PDF set.

In Figs. 16-17 the photon PDF from the MRST2004QED set is also shown for comparison. The MRST2004QED photon PDF is based on a model; an alternative (not publicly available) version of it, in which constituent rather than current quark masses are used as model parameters, has been used [50] to estimate the model uncertainty, though

NNPDF2.3 NLO vs NNPDF2.3QED NLO, at  $Q^2 = 10^4 \text{ GeV}^2$

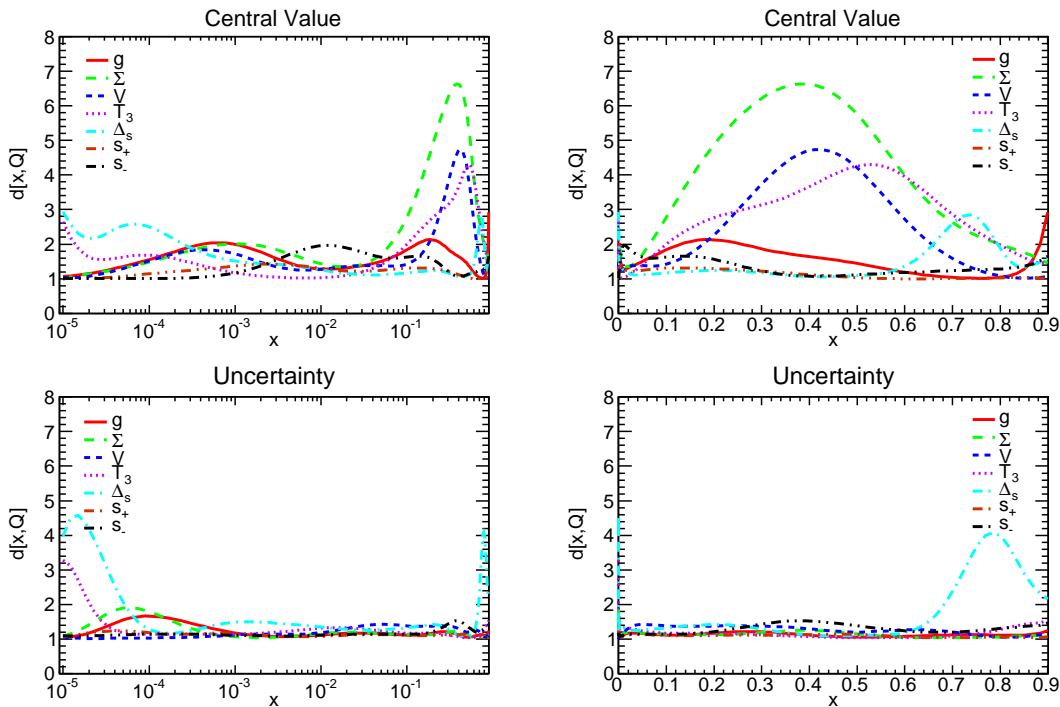


Figure 19: Same as Fig. 18 but now computed at  $Q^2 = 10^4 \text{ GeV}^2$ .

constituent masses are considered to be less appropriate by the authors of Ref. [24]. The MRST2004QED photon turns out to be in good agreement with the central NNPDF2.3QED prediction at medium and large  $x$ , but at small  $x \lesssim 0.03$  it grows more quickly, and for  $x \leq 10^{-2}$  it is larger and well outside the NNPDF2.3QED uncertainty band.

It is also interesting to compare the PDFs from the NNPDF2.3QED and MRST2004QED sets at the level of the parton luminosities which enter the computation of hadronic processes. This comparison is shown in Fig. 20. The two luminosities are in good agreement for invariant masses of the final state  $M_X \sim 100 \text{ GeV}$ , but the agreement is less good for higher or lower final-state masses, with the MRST2004QED rather smaller at high mass and larger at low mass, where, for  $M_X \sim 20 \text{ GeV}$  it is outside the NNPDF2.3QED uncertainty band. As we will see in the next section, these differences translate into differences in the predictions for electroweak processes at the LHC.

So far, we have shown results for the PDFs of the proton. Note, however that, as discussed in Sect. 2, even though we assume that isospin holds at the scale at which PDFs are parametrized, QED corrections to perturbative evolution introduce a violation of the isospin symmetry at all other scales. Therefore, we provide independent NNPDF2.3QED PDF sets for proton and neutron. The size of isospin violation is expected to be comparable to the QED corrections themselves, so very small for quark and gluon distributions but more significant for the photon PDF. The expectation is borne out by Fig. 21 where the ratio of the neutron to the proton PDF at  $Q^2 = 10^4 \text{ GeV}^2$  in NNPDF2.3QED NLO is compared to that in MRST2004QED set. The comparison shows that while the amount

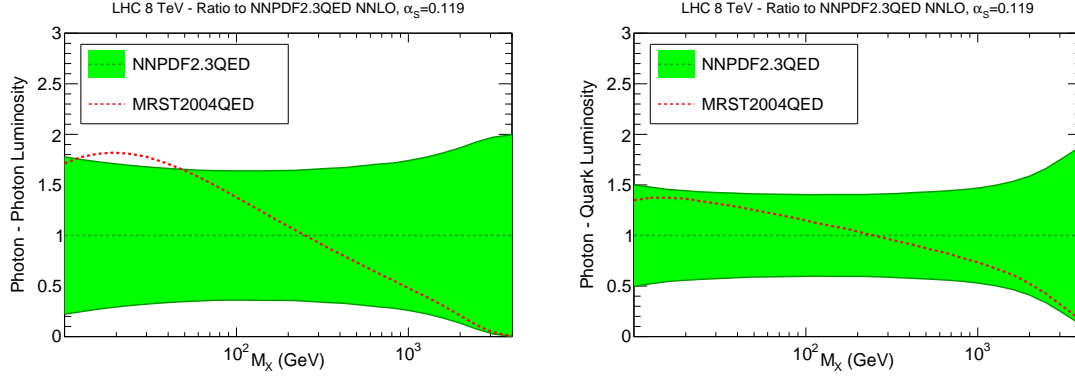


Figure 20: The photon-photon  $\gamma\gamma$  (left) and photon-quark  $\gamma q$  (right) parton luminosities at the LHC 8 TeV computed using MRST2004QED PDFs, shown as a ratio to the NNPDF2.3QED result. The 68% confidence level on the latter is also shown.

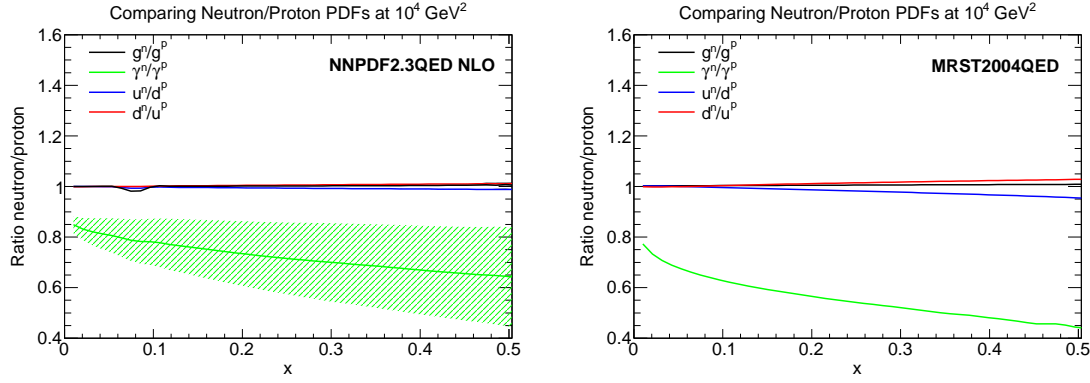


Figure 21: The ratio of the neutron to the proton PDFs in the NNPDF2.3QED NLO set at  $Q^2 = 10^4 \text{ GeV}^2$  (left) and MRST2004QED set (right). Results for the photon, gluon, up and down quark are shown. Error bands correspond to one- $\sigma$  uncertainties.

of isospin violation in the MRST2004QED photon PDF, which had a built-in model of non-perturbative isospin violation, is somewhat larger than our own, especially at large  $x$ , the difference is within the PDF uncertainty, as anticipated in Sect. 2.2. The amount of isospin violation on quark and gluon PDFs is extremely small, on the scale of PDF uncertainties, both for MRST2004QED and NNPDF2.3QED. The same conclusions hold if the NNLO set is used.

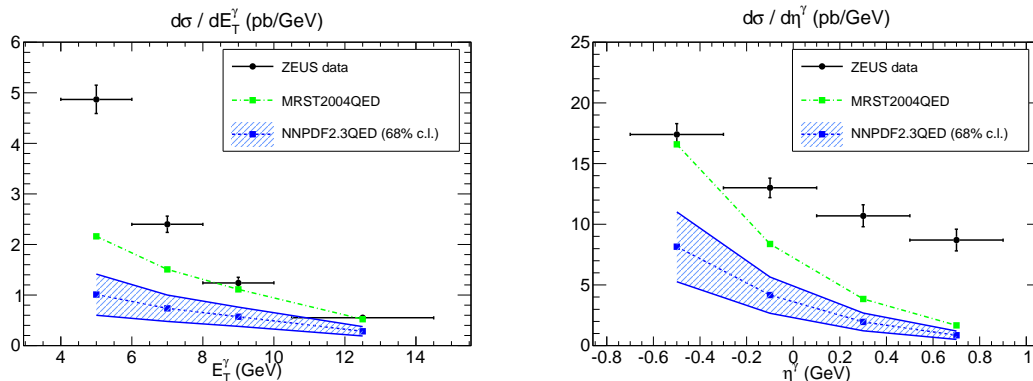


Figure 22: Comparison between the ZEUS data [58] for the photon transverse energy (left) and rapidity (right) distributions in deep-inelastic isolated photon production and the leading log theoretical prediction obtained using NNPDF2.3QED and MRST2004QED PDFs.

## 4 Implications for HERA and LHC phenomenology

As first examples of the use of the NNPDF2.3QED PDF set, we consider now several processes which are sensitive to photon-initiated corrections. In particular, we will discuss direct photon production at HERA, backgrounds for searches for new massive electroweak gauge bosons and  $W$  pair production at small  $p_T$  and large invariant mass.

### 4.1 Direct photon production at HERA

Deep-inelastic isolated photon production provides a direct handle on the photon parton distribution of the proton, through Compton scattering of the incoming electron off the photon component of the proton (see Ref. [59] and references therein). At the leading log level, this  $O(\alpha^2)$  partonic subprocess is the only contribution. In practice, however, the  $O(\alpha^3)$  quark-induced contributions [60] may be comparable (as for the Drell-Yan process discussed in Sect. 3) because of the larger size of the quark distribution. In Ref. [24], the total cross-section for this process computed at the leading log level using MRST2004QED PDFs was shown to be in reasonable agreement with HERA integrated cross sections for prompt photon production data [61].

However, more recent HERA data [58] for the rapidity and transverse energy distribution of the photon do not agree well with either the fixed order [60] or the leading log [24, 59] results for all values of the kinematics, suggesting that a calculation matching the leading-log resummation to the fixed order result would be necessary in order to obtain good agreement. In the absence of such a calculation, we did not use these data for the determination of the photon PDF.

Theoretical predictions obtained using the leading log calculation [24] and the NNPDF2.3QED or MRST2004QED PDF sets are compared in Fig. 22 to the ZEUS data of Ref. [58]. These predictions have been obtained using the code of Ref. [24]. The selection cuts are the same as in [58], namely

$$10 \leq Q^2 \leq 300 \text{ GeV}^2, \quad 4 \leq E_T^\gamma \leq 15 \text{ GeV}, \quad -0.7 \leq \eta^\gamma \leq 0.9. \quad (7)$$

The fact that the prediction is in better agreement with the data at large  $E_T$  is consistent with the expectation that the leading log approximation which is being used is more reliable in this region. However, as already mentioned, a fully matched calculation would be needed in order to consistently combine the leading log and fixed order results.

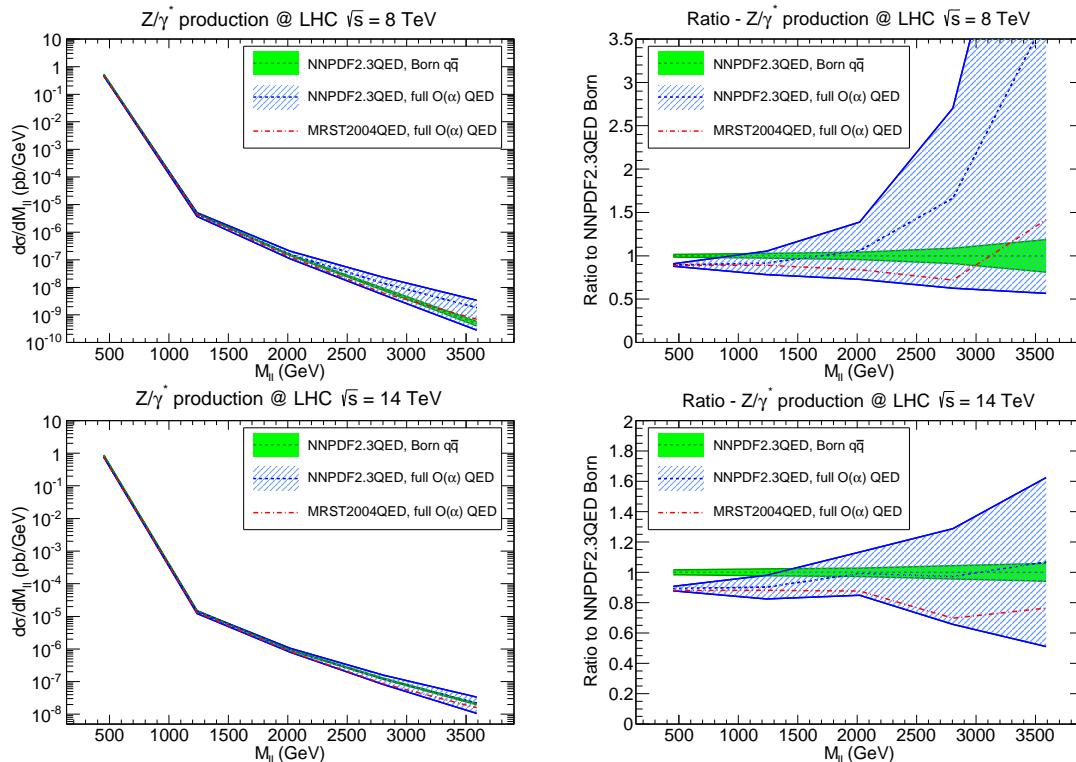


Figure 23: Neutral current Drell-Yan production at the LHC as a function of the invariant mass of the dilepton pair using NNPDF2.3QED and MRST2004QED PDFs. Theoretical predictions for the Born  $q\bar{q}$  and the full  $O(\alpha)$  process (including photon-induced contributions) at the LHC 8 TeV (top) and LHC 14 TeV (bottom), are shown both on an absolute scale (left) or as a ratio to the central value of the Born  $q\bar{q}$  cross section from NNPDF2.3QED.

## 4.2 Searches for new massive electroweak gauge bosons

Heavy electroweak gauge bosons, denoted generically by  $W'$  and  $Z'$ , have been actively searched at the LHC (see e.g. [62–65]), with current limits for  $M_{V'}$  between 1 and 2 TeV depending on the model assumptions. The main background for such searches is the off-resonance production of  $W$  and  $Z$  bosons respectively. At such large invariant masses of the dilepton pair, photon-induced contributions, of the type shown in Figs. 9–10, are potentially large.

We have thus computed the theoretical predictions for high mass off-shell  $W$  and  $Z$  production using NNPDF2.3QED. We have calculated separately the  $q\bar{q}$  initiated Born contributions, the Born term supplemented by photon-initiated processes, and the full set of  $O(\alpha)$  QED corrections, all determined with HORACE (hence using LO QCD theory) and

the various electroweak scheme choices discussed in Sect. 3.2. We have used the following kinematical cuts, roughly corresponding to those used in the ATLAS and CMS searches

$$p_t^l \geq 25 \text{ GeV}, \quad |\eta^\gamma| \leq 2.4, \quad (8)$$

and we have generated enough statistics to properly populate the highest mass bins and reduce the impact of statistical fluctuations. Results are displayed in Fig. 23, for the neutral-current and in Fig. 24 for charged-current dilepton production respectively. They are provided for LHC 8 TeV and LHC 14 TeV, shown both in an absolute scale and as a ratio to the central value of the Born  $q\bar{q}$  cross section from NNPDF2.3QED, using the NLO set.

The contribution from the photon-induced diagrams is generally not negligible. Especially in the neutral current case, in which the photon-induced contribution starts at Born level, the uncertainty induced by the QED corrections in the large invariant mass region is substantial, because the LHC data we used to constrain the photon PDF (recall in particular Tab. 2 and Fig. 11) have little effect there: the uncertainty is of order 20% for  $M_{ll} \sim 1 \text{ TeV}$  at LHC 8 TeV, and it reaches the 50% level for  $M_{ll} \sim 2 \text{ TeV}$ . Of course, for a given value of  $M_{ll}$ , the photon-induced uncertainties decrease when going to 14 TeV, since smaller values of  $x$  are probed, closer to the region of the data used for the current PDF determination.

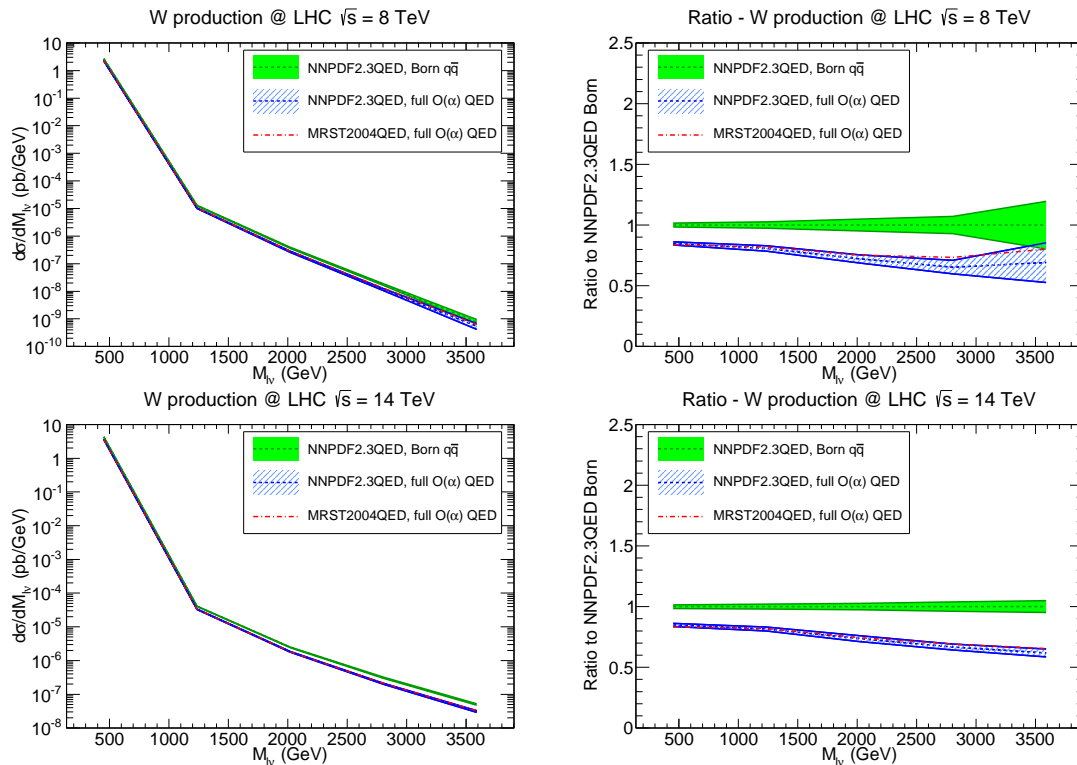


Figure 24: Same as Fig. 23 but for high-mass charged-current production.

Currently, the uncertainty on QED corrections is typically estimated by varying the photon PDF between its MRST2004QED value and zero. Our results suggest that this

might underestimate the size of the photon-induced contribution; it certainly does underestimate the uncertainty related to our current knowledge of it. This follows directly from the behavior of the luminosities of Fig. 20. In order to obtain more reliable exclusion limits for  $Z'$  and  $W'$  at the LHC, a more accurate determination of the photon PDF at large  $x$  might be necessary. This could come from the inclusion in the global PDF fit of new observables that are particularly sensitive to the photon PDF, such as  $W$  pair production, as we now discuss.

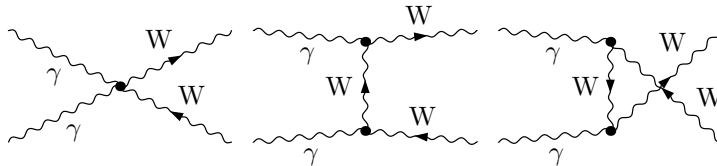


Figure 25: Tree-level diagrams for the LO processes  $\gamma\gamma \rightarrow W^-W^+$ , from Ref. [66].

### 4.3 $W$ pair production at the LHC

The production of pairs of electroweak gauge bosons is important, specifically for the determination of triple and quartic gauge boson couplings [67–69], and it is a significant background to searches [70–74] since several extensions to the Standard Model including warped extra dimensions [75] and dynamical electroweak symmetry-breaking models [76, 77] predict the existence of heavy resonances decaying to pairs of electroweak gauge bosons.

We consider now specifically the production of  $W$  boson pairs for large values of the invariant mass  $M_{WW}$  and moderate values of the transverse momentum  $p_{T,W}$ . Photon-induced contributions to this process start at Born level (see Fig. 25), and their contribution can be substantial, in particular at large values of  $M_{WW}$ . NLO QCD corrections, as well as the formally NNLO but numerically significant gluon-gluon initiated contributions, are known, and available in public codes such as MCFM [78]. Fixed-order electroweak corrections to  $W$  pair production are also known [66], as well as the resummation of large Sudakov electroweak logarithms at NNLL accuracy [79]; a recent review of theoretical calculations is in Ref. [80].

To estimate the impact of photon-induced contributions to  $WW$  production, predictions have been computed with either MRST2004QED or NNPDF2.3QED NLO PDFs. They have been provided by the authors of Ref. [66] using the code and settings of Ref. [66]. In particular, the kinematical cuts in the transverse momentum and rapidity of the  $W$  bosons are

$$p_{T,W} \geq 15 \text{ GeV}, \quad |y_W| \leq 2.5. \quad (9)$$

In Fig. 26 the cross-section for production of a  $W$  pair of mass  $M_{WW} > M_{WW}^{\text{cut}}$  is displayed as a function of  $M_{WW}^{\text{cut}}$ , at the LHC 8 and 14 TeV. The Born  $q\bar{q}$  and  $\gamma\gamma$  initiated contributions are shown (computed using LO QCD), while we refer to Ref. [66] for the full  $O(\alpha)$  electroweak corrections, which depend only weakly on the photon PDF. It

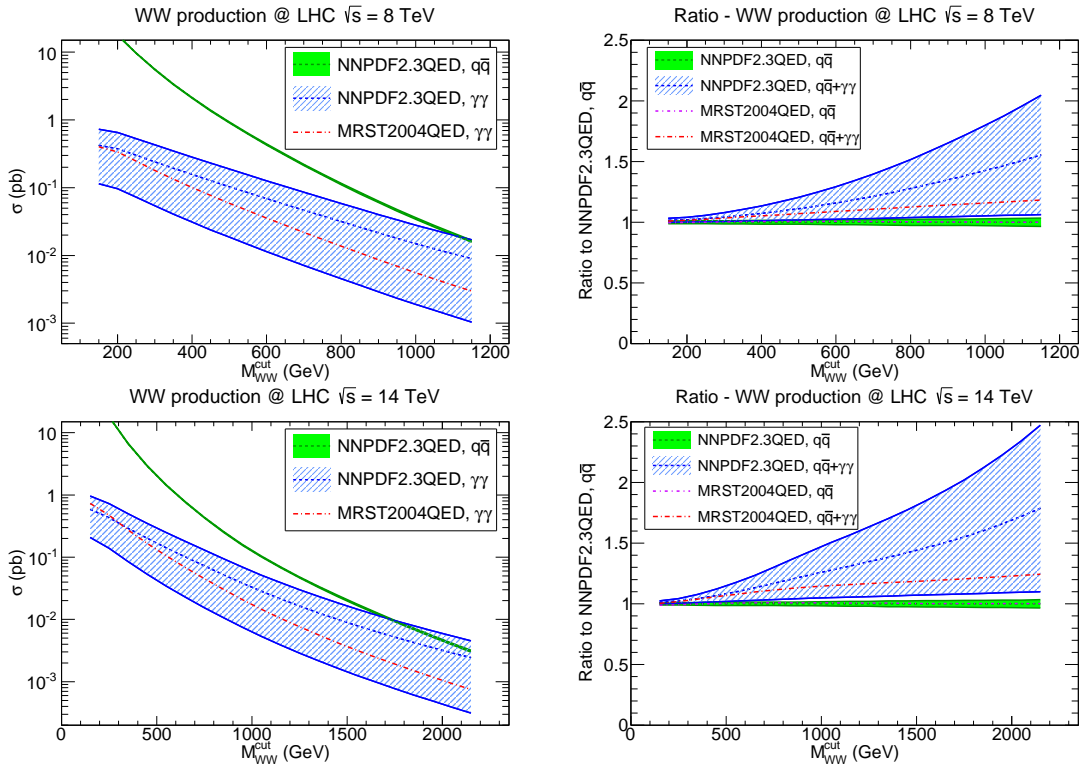


Figure 26: Photon-induced and quark-induced Born-level contributions to the production of a  $W$  pair with mass  $M_{WW} > M_{WW}^{\text{cut}}$  plotted as a function of  $M_{WW}^{\text{cut}}$  at the LHC 8 TeV (top) and LHC 14 TeV (bottom), computed with the code of Ref. [66] and NNPDF2.3QED NLO and MRST2004QED PDFs.

is clear that for large enough values of the mass of the pair the photon-induced contribution becomes increasingly important. Again, the relative size of the results obtained using NNPDF2.3QED or MRST2004QED PDFs can be inferred from the behavior of the luminosities shown in Fig. 20.

As in the case of Fig. 23, the large uncertainties found for large values of  $M_{WW}^{\text{cut}}$  reflect the lack of knowledge on the photon PDF at large  $x \gtrsim 0.1$ . Indeed, in Fig. 27 we display the correlation between the cross section of Fig. 26 and the photon PDF at  $Q^2 = 10^4 \text{ GeV}^2$  as a function of  $x$ , obtained subdividing the range of  $M_{WW}^{\text{cut}}$  of Fig. 26 into 40 bins of equal width, and then computing the correlation for each bin. It is clear that this process is sensitive to the photon PDF at large  $x$ , where the data of Tab. 2 provide little or no constraint (recall Fig. 11). Hence, predictions for  $W$  pair production obtained using MRST2004QED or NNPDF2.3QED should be taken with care: NNPDF2.3QED provides a more conservative estimate of the uncertainties involved, but perhaps overestimates the range of reasonable photon PDF shapes. However, future measurements of this process could be used to pin down the photon PDF at large  $x$ , and thus in turn improve the accuracy of the prediction for very high mass Drell-Yan production discussed in Sect. 4.2 and Fig. 23, and conversely. Of course, in using either, or both of these channels for new physics searches, care should be taken that the sought-for new physics effects are not being hidden in the PDFs themselves, which could be done by introducing suitable kinematic



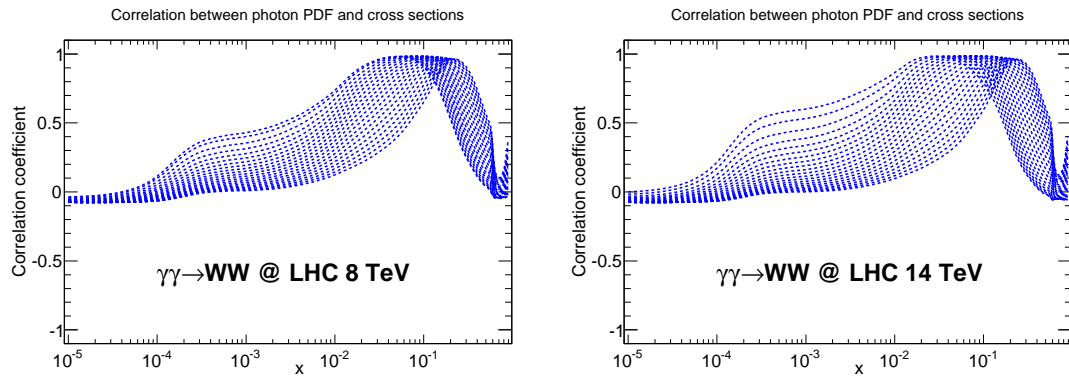


Figure 27: Correlations between the  $W$  pair production cross section of Fig. 26 and the photon PDF from the NNPDF2.3QED NLO set for  $Q = 10^4$  GeV<sup>2</sup>. Each curve corresponds to one of 40 equally spaced bins in which the  $M_{WW}^{\text{cut}}$  range of Fig. 26 has been subdivided.

cuts.

## 5 Conclusions

We have presented a first determination of PDFs with QED corrections and including a photon PDF using NNPDF methodology. The photon PDF is determined by deep-inelastic scattering and neutral- and charged-current Drell-Yan production data from the LHC. The LHC data constrain the photon PDF in the range  $10^{-5} \lesssim x \lesssim 10^{-1}$  at the initial scale  $Q^2 = 2 \text{ GeV}^2$ . In comparison to the previous MRST2004QED set, we also provide PDF uncertainties, and we determine the photon from data, rather than from a model. We find that our central photon PDF is in good agreement with the MRST2004QED result for  $x \gtrsim 0.03$ , but is rather smaller for lower values of  $x$ .

The main shortcoming of our determination of the photon PDF is the lack of experimental information for  $x \gtrsim 0.1$ . This induces substantial uncertainties related to electroweak corrections in processes which are relevant for new physics searches at the LHC, such as high mass gauge boson production and double gauge boson production. This latter process could in turn be used to constrain the large  $x$  photon PDF once accurate LHC data become available.

Now that a first determination of the photon PDF based on data is available, it will be interesting to give a more precise assessment of the impact of QED corrections on precision electroweak measurements at the LHC, such as the determination of the  $W$  mass [81]. A more systematic investigation of processes which may be used to constrain the photon PDF is now in order.

The NNPDF2.3QED PDF sets, proton and neutron, NLO and NNLO, are available from the NNPDF web site,

<http://nnpdf.hepforge.org/>

and through the LHAPDF interface [82]. The list of available new grids is the following:

- NNPDF23\_nlo\_as\_0117\_qed.LHgrid
- NNPDF23\_nlo\_as\_0117\_qed\_neutron.LHgrid
- NNPDF23\_nnlo\_as\_0117\_qed.LHgrid
- NNPDF23\_nnlo\_as\_0117\_qed\_neutron.LHgrid
- NNPDF23\_nlo\_as\_0118\_qed.LHgrid
- NNPDF23\_nlo\_as\_0118\_qed\_neutron.LHgrid
- NNPDF23\_nnlo\_as\_0118\_qed.LHgrid
- NNPDF23\_nnlo\_as\_0118\_qed\_neutron.LHgrid
- NNPDF23\_nlo\_as\_0119\_qed.LHgrid
- NNPDF23\_nlo\_as\_0119\_qed\_neutron.LHgrid
- NNPDF23\_nnlo\_as\_0119\_qed.LHgrid

- `NNPDF23_nnlo_as_0119_qed_neutron.LHgrid`

Note that unlabelled (default) grids refer to the proton.

The NNPDF2.3QED sets are included in LHAPDF 5.9.0 and subsequent releases.

---

### **Acknowledgments**

We are grateful to Alessandro Vicini for discussions about QED corrections and the `HORACE` generator, and Giancarlo Ferrera for assistance with `DYNNLO`; to James Stirling and Robert Thorne for information on `MRST2004QED` set and for providing us with their code for direct photon production in HERA; to Tobias Kasprzik for providing the predictions for  $WW$  production with electroweak corrections using `NNPDF2.3QED`; to Sasha Glazov and Uta Klein for providing information on the ATLAS Drell-Yan measurements; and to Katharina Müller for details on the the LHCb data. We would also like to thank Stefan Dittmaier for discussions about QED and electroweak corrections at the LHC, and for emphasizing the importance of scheme choices in the treatment of QED corrections. S.C. and S.F. are supported by an Italian PRIN 2010 and by a European EIBURS grant. J. R. is supported by a Marie Curie Intra-European Fellowship of the European Community's 7th Framework Programme under contract number PIEF-GA-2010-272515.

## References

- [1] S. Forte, *Acta Phys.Polon.* B41 (2010) 2859, 1011.5247.
- [2] S. Forte and G. Watt, (2013), 1301.6754.
- [3] U. Baur, S. Keller and D. Wackerroth, *Phys.Rev.* D59 (1999) 013002, hep-ph/9807417.
- [4] V. Zykunov, *Eur.Phys.J.direct* C3 (2001) 9, hep-ph/0107059.
- [5] S. Dittmaier and M. Kramer, *Phys.Rev.* D65 (2002) 073007, hep-ph/0109062.
- [6] U. Baur et al., *Phys.Rev.* D65 (2002) 033007, hep-ph/0108274.
- [7] U. Baur and D. Wackerroth, *Phys.Rev.* D70 (2004) 073015, hep-ph/0405191.
- [8] A. Arbuzov et al., *Eur.Phys.J.* C54 (2008) 451, 0711.0625.
- [9] A. Arbuzov et al., *Eur.Phys.J.* C46 (2006) 407, hep-ph/0506110.
- [10] S. Brensing et al., *Phys.Rev.* D77 (2008) 073006, 0710.3309.
- [11] G. Balossini et al., *JHEP* 1001 (2010) 013, 0907.0276.
- [12] C. Carloni Calame et al., *JHEP* 0710 (2007) 109, 0710.1722.
- [13] S. Dittmaier and M. Huber, *JHEP* 1001 (2010) 060, 0911.2329.
- [14] A. Denner et al., *JHEP* 0908 (2009) 075, 0906.1656.
- [15] A. Denner et al., *JHEP* 1106 (2011) 069, 1103.0914.
- [16] A. Denner et al., *Eur.Phys.J.* C73 (2013) 2297, 1211.5078.
- [17] S. Moretti, M. Nolten and D. Ross, *Phys.Rev.* D74 (2006) 097301, hep-ph/0503152.
- [18] S. Dittmaier, A. Huss and C. Speckner, *JHEP* 1211 (2012) 095, 1210.0438.
- [19] W. Bernreuther, M. Fuecker and Z. Si, *Phys.Lett.* B633 (2006) 54, hep-ph/0508091.
- [20] J.H. Kuhn, A. Scharf and P. Uwer, *Eur.Phys.J.* C45 (2006) 139, hep-ph/0508092.
- [21] W. Hollik and M. Kollar, *Phys.Rev.* D77 (2008) 014008, 0708.1697.
- [22] W. Hollik and D. Pagani, *Phys.Rev.* D84 (2011) 093003, 1107.2606.
- [23] J. Kühn, A. Scharf and P. Uwer, (2013), 1305.5773.
- [24] A.D. Martin et al., *Eur. Phys. J.* C39 (2005) 155, hep-ph/0411040.
- [25] R.D. Ball et al., *Nucl.Phys.* B867 (2013) 244, 1207.1303.
- [26] M. Ciafaloni, P. Ciafaloni and D. Comelli, *Phys.Rev.Lett.* 88 (2002) 102001, hep-ph/0111109.

- [27] P. Ciafaloni and D. Comelli, JHEP 0511 (2005) 022, hep-ph/0505047.
- [28] T. Carli et al., Eur.Phys.J. C66 (2010) 503, 0911.2985.
- [29] fastNLO Collaboration, M. Wobisch et al., (2011), 1109.1310.
- [30] The NNPDF Collaboration, R.D. Ball et al., Nucl. Phys. B849 (2011) 112, 1012.0836.
- [31] R.D. Ball et al., Nucl.Phys. B855 (2012) 608, 1108.1758.
- [32] The NNPDF Collaboration, R.D. Ball et al., Nucl. Phys. B809 (2009) 1, 0808.1231.
- [33] A. De Rujula, R. Petronzio and A. Savoy-Navarro, Nucl.Phys. B154 (1979) 394.
- [34] J. Kripfganz and H. Perlt, Z.Phys. C41 (1988) 319.
- [35] J. Blumlein, Z.Phys. C47 (1990) 89.
- [36] V. Bertone, S. Carrazza and J. Rojo, (2013), 1310.1394.
- [37] H. Spiesberger, Phys.Rev. D52 (1995) 4936, hep-ph/9412286.
- [38] M. Roth and S. Weinzierl, Phys.Lett. B590 (2004) 190, hep-ph/0403200.
- [39] M. Dittmar et al., (2009), 0901.2504.
- [40] S. Weinzierl, Comput.Phys.Commun. 148 (2002) 314, hep-ph/0203112.
- [41] K.P. Diener, S. Dittmaier and W. Hollik, Phys.Rev. D72 (2005) 093002, hep-ph/0509084.
- [42] The NNPDF Collaboration, R.D. Ball et al., Nucl.Phys. B874 (2013) 36, 1303.7236.
- [43] G. Altarelli, S. Forte and G. Ridolfi, Nucl. Phys. B534 (1998) 277, hep-ph/9806345.
- [44] The NNPDF Collaboration, R.D. Ball et al., Nucl.Phys. B855 (2012) 153, 1107.2652.
- [45] R.D. Ball et al., JHEP 1304 (2013) 125, 1211.5142.
- [46] The NNPDF Collaboration, R.D. Ball et al., JHEP 05 (2010) 075, 0912.2276.
- [47] J. Londergan and A.W. Thomas, Phys.Lett. B558 (2003) 132, hep-ph/0301147.
- [48] The NNPDF Collaboration, R.D. Ball et al., Nucl. Phys. B838 (2010) 136, 1002.4407.
- [49] LHCb Collaboration, (2012), LHCb-CONF-2012-013.
- [50] ATLAS Collaboration, G. Aad et al., Phys.Rev. D85 (2012) 072004, 1109.5141.
- [51] ATLAS Collaboration, G. Aad et al., (2013), 1305.4192.
- [52] CMS Collaboration, (2013), CMS-PAS-SMP-13-003.
- [53] F. Demartin et al., Phys. Rev. D82 (2010) 014002, 1004.0962.
- [54] S. Alekhin et al., (2011), 1101.0536.

- [55] S. Carrazza, (2013), 1307.1131.
- [56] S. Catani, G. Ferrera and M. Grazzini, JHEP 1005 (2010) 006, 1002.3115.
- [57] R.D. Ball, Nucl.Phys. B796 (2008) 137, 0708.1277.
- [58] ZEUS Collaboration, S. Chekanov et al., Phys.Lett. B687 (2010) 16, 0909.4223.
- [59] A. De Rujula and W. Vogelsang, Phys.Lett. B451 (1999) 437, hep-ph/9812231.
- [60] A. Gehrmann-De Ridder, T. Gehrmann and E. Poulsen, Phys.Rev.Lett. 96 (2006) 132002, hep-ph/0601073.
- [61] ZEUS Collaboration, S. Chekanov et al., Phys.Lett. B595 (2004) 86, hep-ex/0402019.
- [62] CMS Collaboration, S. Chatrchyan et al., JHEP 1208 (2012) 023, 1204.4764.
- [63] CMS Collaboration, S. Chatrchyan et al., Phys.Lett. B701 (2011) 160, 1103.0030.
- [64] CMS Collaboration, S. Chatrchyan et al., JHEP 1105 (2011) 093, 1103.0981.
- [65] ATLAS Collaboration, G. Aad et al., Phys.Rev.Lett. 107 (2011) 272002, 1108.1582.
- [66] A. Bierweiler et al., JHEP 1211 (2012) 093, 1208.3147.
- [67] CMS Collaboration, S. Chatrchyan et al., Phys.Lett. B721 (2013) 190, 1301.4698.
- [68] CMS Collaboration, S. Chatrchyan et al., Phys.Lett. B699 (2011) 25, 1102.5429.
- [69] ATLAS Collaboration, G. Aad et al., (2012), 1210.2979.
- [70] CMS Collaboration, S. Chatrchyan et al., (2012), 1212.1910.
- [71] CMS Collaboration, S. Chatrchyan et al., JHEP 1302 (2013) 036, 1211.5779.
- [72] CMS Collaboration, S. Chatrchyan et al., Phys.Rev.Lett. 109 (2012) 141801, 1206.0433.
- [73] ATLAS Collaboration, G. Aad et al., (2013), 1305.0125.
- [74] ATLAS Collaboration, G. Aad et al., Phys.Lett. B718 (2013) 860, 1208.2880.
- [75] L. Randall and R. Sundrum, Phys.Rev.Lett. 83 (1999) 4690, hep-th/9906064.
- [76] J. Andersen et al., Eur.Phys.J.Plus 126 (2011) 81, 1104.1255.
- [77] E. Eichten and K. Lane, Phys.Lett. B669 (2008) 235, 0706.2339.
- [78] J.M. Campbell, R.K. Ellis and C. Williams, JHEP 1107 (2011) 018, 1105.0020.
- [79] J. Kuhn et al., JHEP 1106 (2011) 143, 1101.2563.
- [80] J. Baglio, L.D. Ninh and M.M. Weber, (2013), 1307.4331.
- [81] G. Bozzi, J. Rojo and A. Vicini, Phys.Rev. D83 (2011) 113008, 1104.2056.
- [82] D. Bourilkov, R.C. Group and M.R. Whalley, (2006), hep-ph/0605240.